

# Nighttime measurements of HO<sub>x</sub> during the RONOCO project and analysis of the sources of HO<sub>2</sub>

H.M. Walker<sup>1</sup>, D. Stone<sup>1</sup>, T. Ingham<sup>1,2</sup>, S. Vaughan<sup>1</sup>, B. Bandy<sup>3</sup>, M. Cain<sup>4,5</sup>, R.L. Jones<sup>4</sup>, O.J. Kennedy<sup>4</sup>, M. McLeod<sup>4</sup>, B. Ouyang<sup>4</sup>, J. Pyle<sup>4,5</sup>, S. Bauguitte<sup>6,7</sup>, G. Forster<sup>8,9</sup>, M.J. Evans<sup>10,11</sup>, J.F. Hamilton<sup>10</sup>, J.R. Hopkins<sup>10,11</sup>, J.D. Lee<sup>10,11</sup>, A.C. Lewis<sup>10,11</sup>, R.T. Lidster<sup>10</sup>, S. Punjabi<sup>10,11</sup>, W.T. Morgan<sup>12,13</sup>, D.E. Heard<sup>1,2</sup>

[1] {School of Chemistry, University of Leeds, Leeds, UK}

[2] {National Centre for Atmospheric Science, University of Leeds, Leeds, UK}

[3] {School of Environmental Sciences, University of East Anglia, Norwich, UK}

[4] {Department of Chemistry, University of Cambridge, Cambridge, UK}

[5] {National Centre for Atmospheric Science, University of Cambridge, Cambridge, UK}

[6] {Facility for Airborne Atmospheric Measurements (FAAM), Cranfield University, Cranfield, UK}

[7] {National Centre for Atmospheric Science, FAAM, Cranfield University, Cranfield, UK}

[8] {Centre for Ocean and Atmospheric Sciences, School of Environmental Sciences, University of East Anglia, Norwich, UK}

[9] {National Centre for Atmospheric Science, University of East Anglia, Norwich, UK}

[10] {Wolfson Atmospheric Chemistry Laboratories, Department of Chemistry, University of York, York, UK}

[11] {National Centre for Atmospheric Science, University of York, York, UK}

[12] {School of Earth, Atmospheric and Environmental Sciences, University of Manchester, Manchester, UK}

[13] {National Centre for Atmospheric Science, University of Manchester, Manchester, UK}

Correspondence to: D. E. Heard (d.e.heard@leeds.ac.uk)



28

29 **Abstract**

30 Measurements of the radical species OH and HO<sub>2</sub> were made using the Fluorescence Assay  
 31 by Gas Expansion (FAGE) technique during a series of nighttime and daytime flights over  
 32 the UK in summer 2010 and winter 2011. OH was not detected above the instrument's 1σ  
 33 limit of detection during any of the nighttime flights or during the winter daytime flights,  
 34 placing upper limits on [OH] of  $1.8 \times 10^6$  molecule cm<sup>-3</sup> and  $6.4 \times 10^5$  molecule cm<sup>-3</sup> for the  
 35 summer and winter flights, respectively. HO<sub>2</sub> reached a maximum concentration of  $3.2 \times 10^8$   
 36 molecule cm<sup>-3</sup> (13.6 pptv) during a nighttime flight on 20<sup>th</sup> July 2010, when the highest  
 37 concentrations of NO<sub>3</sub> and O<sub>3</sub> were also recorded. Analysis of the rates of reaction of OH, O<sub>3</sub>,  
 38 and the NO<sub>3</sub> radical with measured alkenes indicates that the summer nighttime troposphere  
 39 can be as important for the processing of VOCs as the winter daytime troposphere. Analysis  
 40 of the instantaneous rate of production of HO<sub>2</sub> from the reactions of O<sub>3</sub> and NO<sub>3</sub> with alkenes  
 41 has shown that, on average, reactions of NO<sub>3</sub> dominated nighttime production of HO<sub>2</sub> during  
 42 summer, and reactions of O<sub>3</sub> dominated nighttime HO<sub>2</sub> production during winter.

43

44 **1 Introduction**

45 Trace gases emitted into the atmosphere, including pollutants and greenhouse gases, are  
 46 removed primarily by oxidation. The hydroxyl radical, OH, is the most important oxidising  
 47 species in the daytime troposphere, reacting with numerous species including volatile organic  
 48 compounds (VOCs), CO, SO<sub>2</sub>, and long-lived anthropogenic halogenated compounds. During  
 49 the day, primary production of OH (i.e. initialisation of the radical chain) occurs  
 50 predominantly via photolysis of ozone at  $\lambda \leq 340$  nm followed by reaction of the resulting  
 51 electronically excited oxygen atom, O(<sup>1</sup>D), with water vapour. The OH-initiated oxidation of  
 52 VOCs leads to the production of the hydroperoxy radical, HO<sub>2</sub>, and together the two radicals  
 53 form the HO<sub>x</sub> family. A key reaction in the conversion of OH to HO<sub>2</sub> is the reaction with CO:



56 Reaction of OH with VOCs results in the production of organic peroxy radicals, RO<sub>2</sub>:





59 Reactions of  $HO_2$  and  $RO_2$  with  $NO$  propagate the  $HO_x$  radical chain, regenerating  $OH$ :



63 The production of  $OH$  through photolysis of ozone (and other species at longer wavelengths)  
 64 is limited to daylight hours, and oxidation of trace gases at night proceeds through alternative  
 65 mechanisms. Two mechanisms are known to initiate  $HO_x$  radical chemistry and oxidation  
 66 chemistry at night: ozonolysis of alkenes, and reactions of the nitrate radical,  $NO_3$ , with  
 67 alkenes.

68 Reactions of ozone with alkenes occur via addition of ozone to the double bond to form a  
 69 five-membered ring called a primary ozonide. The primary ozonide decomposes to form one  
 70 of two possible pairs of products, each pair consisting of a carbonyl compound and a  
 71 vibrationally- and rotationally-excited carbonyl oxide termed a Criegee intermediate (CI).  
 72 The simplest gas-phase CI,  $CH_2OO$ , and the alkyl-substituted  $CH_3CHOO$ , have been  
 73 observed directly by photoionisation mass spectrometry (Taatjes et al., 2008; Beames et al.,  
 74 2012; Taatjes et al., 2012; Welz et al., 2012; Beames et al., 2013; Taatjes et al., 2013; Stone  
 75 et al., 2014a), by infrared absorption spectroscopy (Su et al., 2013), and by microwave  
 76 spectroscopy (Nakajima and Endo, 2013, 2014). Excited CIs may be stabilised by collision  
 77 with surrounding molecules (Donahue et al., 2011; Drozd and Donahue, 2011), or may  
 78 undergo isomerisation or decomposition to yield products including  $OH$ ,  $H$ , and subsequently  
 79  $HO_2$  (Paulson and Orlando, 1996; Kroll et al., 2001a; Kroll et al., 2001b; Kroll et al., 2002;  
 80 Johnson and Marston, 2008). Stabilised CIs (SCIs) are known to react with a variety of  
 81 compounds, including  $H_2O$ ,  $NO_2$ ,  $SO_2$ , and a variety of organic compounds (e.g. Mauldin III  
 82 et al., 2012; Taatjes et al., 2012; Ouyang et al., 2013; Taatjes et al., 2013; Stone et al., 2014a;  
 83 Taatjes et al., 2014). There is experimental evidence for the formation of  $OH$  from thermal  
 84 decomposition of SCIs, on a much longer timescale than the decomposition or isomerisation  
 85 of excited CIs (Kroll et al., 2001a; Kroll et al., 2001b). The  $OH$  produced through these  
 86 ozonolysis mechanisms will proceed to oxidise other VOC species. Criegee intermediates  
 87 formed in the ozonolysis of alkenes are known to be an important source of  $HO_x$  during the  
 88 day and at night (Paulson and Orlando, 1996; Donahue et al., 1998; Kanaya et al., 1999;

Salisbury et al., 2001; Geyer et al., 2003; Ren et al., 2003a; Heard et al., 2004; Harrison et al., 2006; Ren et al., 2006; Sommariva et al., 2007). The gas-phase ozonolysis of unsaturated VOCs, and in particular the role and subsequent chemistry of the Criegee intermediate, have been reviewed in detail by Johnson and Marston (2008), Donahue et al. (2011), Vereecken and Francisco (2012), and Taatjes et al. (2014).

Another key nighttime oxidant, NO<sub>3</sub>, is formed primarily by reaction of NO<sub>2</sub> with ozone. NO<sub>3</sub> reacts with a range of species in the troposphere, and its reaction with alkenes is known to be an important nighttime oxidation mechanism (Salisbury et al., 2001; Geyer et al., 2003; Sommariva et al., 2007; Emmerson and Carslaw, 2009; Brown et al., 2011). The reaction between NO<sub>3</sub> and an alkene proceeds primarily via addition to a double bond, to form a nitrooxyalkyl radical, R-ONO<sub>2</sub>. At atmospheric pressure, the main fate of the nitrooxyalkyl radical is reaction with O<sub>2</sub> (Berndt and Böge, 1994) to produce a nitrooxyalkyl peroxy radical, O<sub>2</sub>-R-ONO<sub>2</sub>. The nitrooxyalkyl peroxy radical can react with NO<sub>2</sub>, HO<sub>2</sub>, RO<sub>2</sub>, NO and NO<sub>3</sub>, of which the latter two reactions lead to formation of the nitrooxyalkoxy radical, O-R-ONO<sub>2</sub>. The nitrooxyalkoxy radical can undergo isomerisation, decomposition, or reaction with O<sub>2</sub>. Reaction with O<sub>2</sub>, analogous to the reaction of organic alkoxy radicals, yields HO<sub>2</sub>:



Thus, nighttime oxidation of hydrocarbons by NO<sub>3</sub> leads to production of HO<sub>2</sub>. Reaction of HO<sub>2</sub> with NO (Reaction (R7)), O<sub>3</sub> and NO<sub>3</sub> can generate OH:



Atkinson and Arey (2003) published a detailed review of tropospheric degradation of VOCs, including reaction with O<sub>3</sub> and NO<sub>3</sub>. A comprehensive review of nighttime radical chemistry is given by Brown and Stutz (2012).

The oxidising capacity of the nocturnal troposphere is thought to be controlled by the reactions described above, with a limited role for OH and HO<sub>2</sub> due to the absence of their photolytic sources. Oxidation of VOCs at night can have significant effects on daytime air quality and tropospheric ozone production (Brown et al., 2004; Brown et al., 2006; Wong and Stutz, 2010; Brown et al., 2011). Several field measurement campaigns have involved nighttime measurements of OH, HO<sub>2</sub>, RO<sub>2</sub>, and NO<sub>3</sub> (see Table 1), and have highlighted the importance of the vertical profile of nighttime radical concentrations and chemistry (Geyer

and Stutz, 2004a, b; Stutz et al., 2004; Volkamer et al., 2010), but prior to the current work there had been no aircraft-based studies of nighttime chemistry involving measurements of both  $\text{NO}_3$  and  $\text{HO}_2$ , to enable vertical profiling of the lower atmosphere and full evaluation of the nocturnal radical budget. Table 1 gives details of some previous measurements and modelling of nighttime  $\text{HO}_x$  concentrations in polluted or semi-polluted environments. Highlights from these studies are discussed here, with particular attention paid to those involving measurements of  $\text{HO}_x$ ,  $\text{NO}_3$ , and  $\text{O}_3$ , and in which the contributions made by  $\text{O}_3$  and  $\text{NO}_3$  to nighttime radical chemistry have been considered.

Geyer et al. (2003) report radical measurements and modelling from the 1998 Berliner Ozone Experiment (BERLIOZ). Measurements of  $\text{NO}_3$ ,  $\text{RO}_2$ ,  $\text{HO}_2$  and  $\text{OH}$  were made by matrix isolation electron spin resonance (MIESR), chemical amplification (CA), and laser-induced fluorescence (LIF) spectroscopy at a site approximately 50 km from Berlin.  $\text{HO}_2$  was detected at night with concentrations frequently as high as  $5 \times 10^7 \text{ molecule cm}^{-3}$  (approximately 2 pptv), and an average concentration of  $1 \times 10^8 \text{ molecule cm}^{-3}$  over one hour (02:00 to 03:00) of nocturnal measurements during an intensive period of the study (Holland et al., 2003).  $\text{OH}$  was usually below the limit of detection of the LIF instrument ( $3.5 \times 10^5 \text{ molecule cm}^{-3}$ ). Modelling revealed that nitrate radical reactions with terpenes were responsible for producing 53 % of  $\text{HO}_2$  and 36 % of  $\text{OH}$  radicals in the night, with ozonolysis accounting for production of the remaining 47 % of  $\text{HO}_2$  and 64 % of  $\text{OH}$  radicals. A positive linear correlation between  $\text{RO}_2$  and  $\text{NO}_3$  was observed and was reproduced by the model.

Reactions of  $\text{O}_3$  with alkenes were found to be responsible for the majority of formation of  $\text{OH}$  during the winter PUMA (Pollution of the Urban Midlands Atmosphere) campaign (a low photolysis urban environment) (Heard et al., 2004; Emmerson et al., 2005; Harrison et al., 2006). Measurements of  $\text{OH}$ ,  $\text{HO}_2$  and  $\text{RO}_2$  were unavailable at night, but model-predicted values of these radicals were used to calculate that 90 % of nighttime initiation via  $\text{HO}_2$  was from  $\text{O}_3$  reactions. Without measurements of  $\text{NO}_3$  during the campaign, there was no estimate of its contribution to radical initiation.

Modelling results from the MCMA-2003 (Mexico City) field campaign (Volkamer et al., 2010) indicate that nighttime radical production at roof-top level (approximately 16 m above the ground) was dominated by ozonolysis of alkenes, and that reactions of  $\text{NO}_3$  with alkenes played only a minor role. The measurement site was located in a polluted urban environment, with high levels of  $\text{NO}$ ,  $\text{NO}_2$  and  $\text{O}_3$ .  $\text{NO}_3$  was observed at a maximum concentration of 50

pptv during the night at a mean height above the ground of 70 m. Roof-top level concentrations of  $\text{NO}_3$  were estimated using a linear scaling factor calculated from the observed  $\text{O}_3$  vertical gradient, and were found to be, on average, 3 times lower than the concentrations measured at 70 m. This predicted vertical gradient accounts for the relative unimportance of  $\text{NO}_3$  reactions in radical initiation at roof-top level. Propagation of  $\text{RO}_2$  radicals to  $\text{HO}_2$  and  $\text{OH}$ , by reaction with  $\text{NO}_3$ , was found to be negligible.

The 2006 Texas Air Quality Study (TexAQS) involved a series of nighttime flights onboard the NOAA P-3 aircraft over Houston, Texas, and along the Gulf Coast (Brown et al., 2011). Loss rates and budgets of  $\text{NO}_3$  and highly reactive VOCs were calculated, but there were no measurements of  $\text{OH}$ ,  $\text{HO}_2$  and  $\text{RO}_2$  during the flights. Budgets for  $\text{NO}_3$  show that it was lost primarily through reactions with unsaturated VOCs, but the contribution to  $\text{NO}_3$  loss through reaction with peroxy radicals was uncertain because of the lack of direct measurements of  $\text{RO}_2$  during the flights.  $\text{NO}_3$  dominated VOC oxidation, being 3 to 5 times more important than  $\text{O}_3$ .

In summary,  $\text{NO}_3$  and  $\text{O}_3$  have both been found to dominate radical initiation in the nighttime troposphere, and in some situations the two mechanisms were found to be equally important. The relative importance of  $\text{O}_3$ - and  $\text{NO}_3$ -initiated oxidation depends on the availability of  $\text{NO}_3$ , which is determined by the amount of  $\text{NO}_x$  present in the atmosphere and the ratio of  $\text{NO}$  to  $\text{NO}_2$ , and the concentration and species distribution of VOCs (Bey et al., 2001; Geyer et al., 2003). A modelling study by Bey et al. (2001) suggests that nocturnal radical initiation is driven by alkene ozonolysis in urban environments or in environments with low  $\text{NO}_x$  concentrations, while both  $\text{O}_3$  and  $\text{NO}_3$  contribute to radical initiation in rural environments with moderate  $\text{NO}_x$  levels. It is expected that  $\text{NO}_3$  dominates nocturnal radical initiation in air masses containing sufficient  $\text{NO}_2$  and  $\text{O}_3$  for  $\text{NO}_3$  production while being deprived of  $\text{NO}$  (e.g. air masses downwind of urban areas). Geyer and Stutz (2004b) have found that the effects of suppressed mixing in the nocturnal boundary layer can also control whether  $\text{NO}_3$  or  $\text{O}_3$  dominates nighttime radical chemistry.

In this paper we report airborne measurements of  $\text{OH}$  and  $\text{HO}_2$  made during the RONOCO (ROle of Nighttime chemistry in controlling the Oxidising Capacity of the atmosphere) and SeptEx (September Experiment) projects in 2010 and 2011. The rates of reaction between  $\text{O}_3$ ,  $\text{NO}_3$ , and  $\text{OH}$  with the alkenes measured during the flights are investigated. Analysis of radical production from the nighttime reactions of  $\text{O}_3$  and  $\text{NO}_3$  with alkenes is also given. Comparisons are made between the daytime and nighttime chemistry studied, and between

the summer and winter measurement periods. Details and results of a box modelling study, and comparison to the observations, are given by Stone et al. (2014b).

## **2 Details of the RONOCO and SeptEx fieldwork**

RONOCO is a NERC-funded consortium project aimed at improving our understanding of the mechanisms and impact of nocturnal oxidation chemistry over the UK. The RONOCO fieldwork consisted of two measurement campaigns, in July 2010 and January 2011. An additional fieldwork period, SeptEx, was conducted in September 2010. The RONOCO and SeptEx flights were conducted onboard the BAe-146 research aircraft operated by the Facility for Airborne Atmospheric Measurements (FAAM). Both field measurement campaigns were based at East Midlands Airport (52.8° N, 1.3° W) in the UK. During RONOCO the majority of the flying took place at night, with occasional flights beginning or ending in daylight hours to study chemical behaviour at dusk and dawn. Flights during SeptEx were mainly during the day, providing a useful comparison to the nocturnal chemistry.

Flights were conducted between altitudes of 50 m and 6400 m, above the UK and the North Sea. Figure 1 shows the flight tracks during the summer, SeptEx, and winter measurements coloured by altitude. Measurements of OH and HO<sub>2</sub> were made using the University of Leeds aircraft-based Fluorescence Assay by Gas Expansion (FAGE) instrument. A suite of supporting measurements, including CO, O<sub>3</sub>, NO, H<sub>2</sub>O, VOCs, NO<sub>3</sub>, and HCHO, were made during the flights and have been used in the current work. Table 2 summarises the techniques used to measure these species.

Air mass histories for each flight have been calculated using the UK Met Office Numerical Atmospheric-dispersion Modelling Environment (NAME). NAME is a three-dimensional Lagrangian particle dispersion model (Jones et al., 2007) which is run here using the UK Meteorological Office's Unified Model meteorological fields. Model 'particles', restricted to a 300 m deep layer from the surface, were released along the flight path and were tracked backwards through the modelled atmosphere. Model particle densities were integrated over 24 h periods, beginning at 24, 48, 72, and 96 hours before each flight. The resulting 'footprint' maps show the regions where the measured air has been in contact with the surface over the 4 days preceding a flight. An example is shown in Fig. 2, which shows model particle densities integrated over the 24 hour period beginning 48 hours prior to flight B535. The majority of the summer flights were characterised by air masses originating from

the west and south west of the UK, having Atlantic or continental European influences. The SeptEx flights were predominantly influenced by air masses from the north-east, east, and south-east of the UK, with northern European influences. The winter flights were mainly characterised by air masses arriving from the west of the UK, bringing Atlantic influences.

Table 3 gives mean and maximum mixing ratios of CO, O<sub>3</sub>, NO, and NO<sub>2</sub> measured during RONOCO and SeptEx. The mean mixing ratios of NO measured during the summer RONOCO flights are much lower than ground-based nighttime measurements (e.g. 1.0 ppbv during TORCH (Emmerson and Carslaw, 2009), 0–20 ppbv during PMTACS-NY, (Ren et al., 2006)), but are comparable with previous airborne nighttime measurements (e.g. < 30 pptv during TexAQS (Brown et al., 2011)). Mean values of NO up to 14 pptv were reported by Salisbury et al. (2001) for semi-polluted air masses sampled at Mace Head. These comparisons indicate that the RONOCO and SeptEx flights enabled sampling of air masses generally removed from the influence of NO in fresh surface emissions. Table 3 also highlights the unusual chemical conditions encountered during flight B537 on 20<sup>th</sup> July 2010, discussed further in Sect. 4.1. Nighttime altitude profiles of NO<sub>3</sub>, O<sub>3</sub>, *trans*-2-butene, and propene (the latter two being illustrative of the alkenes measured) are given in Fig. 3.

### 3 Experimental

#### 3.1 The Leeds FAGE aircraft instrument

The University of Leeds Aircraft FAGE instrument has been described in detail by Commane et al. (2010). A brief description is given here. The instrument, which was designed specifically for use onboard the FAAM BAe-146 research aircraft (Floquet, 2006), is housed in two double-width 19 inch aircraft racks, with the inlet, detection cells, and pump set being separate to the two racks. Ambient air is sampled through a 0.7 mm diameter ‘pinhole’ into a cylindrical inlet (length = 50 cm, diameter = 5 cm) which extends through a window blank on the starboard side of the aircraft.

Downstream of the inlet are two low pressure fluorescence cells positioned in series, the first for detection of OH and the second for detection of HO<sub>2</sub>. During the RONOCO and SeptEx flights the pressure inside the cells ranged from 1.9 Torr at ground level to 1.2 Torr at 6 km.

Laser light at  $\lambda \sim 308$  nm is generated by a diode-pumped Nd:YAG-pumped tunable Ti:Sapphire laser (Photonics Industries DS-532-10 and TU-UV-308nm) and delivered to the

fluorescence cells via optical fibres, on an axis perpendicular to the gas flow. A small fraction of the Ti:Sapphire second harmonic ( $\lambda = 462$  nm) is directed to the probe of a wavemeter to enable measurement of the laser wavelength to within 0.001 nm. A UV photodiode is positioned opposite the laser input arm on each fluorescence cell to measure laser power.

The sampled air forms a supersonic gas expansion beam in which the rate of collision between OH radicals and ambient air molecules is reduced. The OH fluorescence lifetime is therefore extended to several hundred nanoseconds, significantly longer than the laser pulse, so that the measured signal can be temporally discriminated from laser scattered light. OH is excited from its ground state,  $X^2\Pi_i(v''=0)$ , to its first electronically excited state,  $A^2\Sigma^+(v'=0)$ , at  $\lambda \sim 308$  nm. The resulting on-resonance fluorescence is detected by a UV-sensitive channel photomultiplier tube on an axis perpendicular to both the gas flow and the laser light. HO<sub>2</sub> is detected by titration with an excess of NO (Reaction (R7)), the resulting OH being detected as described.

The FAGE instrument was calibrated prior to and following each field measurement period, using a well-established method (Edwards et al., 2003; Faloon et al., 2004; Commane et al., 2010). Light at  $\lambda = 184.9$  nm from a mercury pen-ray lamp photolyses water vapour in a flow of synthetic air inside an aluminium flow tube, generating OH and HO<sub>2</sub> at known concentrations. The aircraft FAGE instrument's limit of detection (LOD) for OH and HO<sub>2</sub> is determined by the instrument's sensitivity and the standard deviation of the background signal. During the RONOCO and SeptEx fieldwork the  $1\sigma$  LOD for a 5 minute averaging period ranged between 0.64 and  $1.8 \times 10^6$  molecule cm<sup>-3</sup> for OH and between 5.9 and  $6.9 \times 10^5$  molecule cm<sup>-3</sup> for HO<sub>2</sub>.

### 3.2 RO<sub>2</sub>-based interference in FAGE measurements of HO<sub>2</sub>

It has recently been shown that reaction of alkene-derived  $\beta$ -hydroxyalkyl peroxy radicals, RO<sub>2</sub>, with NO inside the HO<sub>2</sub> detection cell, can lead to interference in FAGE HO<sub>2</sub> measurements (Fuchs et al., 2011; Whalley et al., 2013). The magnitude of the interference depends on the parent alkene, the residence time and mean temperature inside the cell, and the amount of NO injected. The interference therefore depends on the chemical environment and differs between FAGE instruments. In view of this, the University of Leeds ground-based and aircraft FAGE instruments have been tested for RO<sub>2</sub> interference. Thorough descriptions of the ground-based experimental method and results, and the results of a modelling study,



are given by Whalley et al. (2013). The strongest interference in the aircraft instrument measurements was observed for ethene-derived RO<sub>2</sub>, amounting to an increase of  $39.7 \pm 4.8$  % in the observed HO<sub>2</sub> signal, with a cell pressure of 1.8 Torr, an estimated detection cell temperature of 255 K (obtained from rotational excitation spectra performed previously), and  $[\text{NO}]_{\text{cell}} = 10^{14}$  molecule cm<sup>-3</sup>.

Whalley et al. (2013) show that the chemistry responsible for the observed interferences is well known, and that a model using the Master Chemical Mechanism (MCM, version 3.2: Jenkin et al., 1997; Saunders et al., 2003; Bloss et al., 2005, via <http://mcm.leeds.ac.uk/MCM>) can reproduce the interferences once tuned to the conversion efficiency of HO<sub>2</sub> to OH in the FAGE detection cell. Accordingly, Stone et al. (2014b) have applied the results of the ethene-derived RO<sub>2</sub> interference testing in a modelling study to assess the effect of the interference on the HO<sub>2</sub> measurements made during the RONOCO and SeptEx campaigns. A box model using a detailed MCM scheme was used to calculate a total potential interference in the RONOCO HO<sub>2</sub> measurements. The model was constrained to the conditions in the detection cell (1.8 Torr, 255 K,  $[\text{NO}] \sim 10^{14}$  molecule cm<sup>-3</sup>). Equal concentrations of HO<sub>2</sub> and  $\sum \text{RO}_2$  (sum of all peroxy radicals in the MCM generated from the parent hydrocarbon) were used to initialise the model. The model run time was varied until the model-predicted interference from ethene-derived RO<sub>2</sub> radicals was equal to the experimentally determined interference, thereby tuning the model to the conversion efficiency of HO<sub>2</sub> to OH. An interference factor,  $f$ , was calculated for each RO<sub>2</sub> in the MCM as follows:

$$f = \frac{[\text{OH}]_{\text{HO}_2 + \text{RO}_2} - [\text{OH}]_{\text{HO}_2}}{[\text{OH}]_{\text{HO}_2}} \quad (1)$$

where  $[\text{OH}]_{\text{HO}_2 + \text{RO}_2}$  and  $[\text{OH}]_{\text{HO}_2}$  are the modelled concentrations of OH produced from the reactions of RO<sub>2</sub> and HO<sub>2</sub>, and the concentration from HO<sub>2</sub> alone, respectively. The greatest interference was calculated to come from isoprene-derived peroxy radicals, followed by aromatic compounds and C<sub>2</sub> to C<sub>5</sub> alkenes. The smallest modelled interference is from the C<sub>1</sub> to C<sub>3</sub> alkanes. The interference factors were applied to model-predicted RO<sub>2</sub> speciation and concentrations for the RONOCO flights. Model-predicted RO<sub>2</sub> species were dominated by CH<sub>3</sub>O<sub>2</sub> (33 %;  $f = 1.1$  %) and HO<sub>2</sub> (24 %;  $f = 0.0$  %), with smaller contributions from RO<sub>2</sub> derived from *iso*-butene (12 %;  $f = 0.5$  %), *cis*-2-butene and *trans*-2-butene (10 %;  $f = 0.05$  %), and isoprene (2 %;  $f = 7.6$  %). RO<sub>2</sub> species with high interference factors were a minor

component of the total RO<sub>2</sub>. A modelled value of HO<sub>2</sub> including the total potential interference, HO<sub>2</sub><sup>\*</sup>, was calculated using:

$$[\text{HO}_2^*] = [\text{HO}_2]_{\text{mod}} + f[\text{RO}_2]_{\text{mod}} \quad (2)$$

Direct comparison between modelled values of [HO<sub>2</sub><sup>\*</sup>] and the FAGE-measured values of [HO<sub>2</sub>] was therefore made possible. The model-predicted interference during the RONOCO campaign is described by  $[\text{HO}_2^*] = 1.15[\text{HO}_2] + 2 \times 10^5 \text{ molecule cm}^{-3}$ . The average model-predicted interference in the HO<sub>2</sub> measurements is 14 %. The HO<sub>2</sub> measurements made during RONOCO and SeptEx were not adjusted since speciated RO<sub>2</sub> measurements were not available. The measurements are hereafter referred to as HO<sub>2</sub><sup>\*</sup>.

The magnitude of the RO<sub>2</sub> interference can be reduced by reducing the concentration of NO in the detection cell. This also reduces the instrument sensitivity to HO<sub>2</sub>. Since conversion of RO<sub>2</sub> to OH requires at least two NO molecules, while conversion of HO<sub>2</sub> requires only one molecule, the ratio of HO<sub>2</sub> signal to RO<sub>2</sub> signal can be made favourable by reducing [NO] (Whalley et al., 2013). This effect has been investigated for the ground-based instrument, and will be investigated for the aircraft instrument prior to future HO<sub>x</sub> measurement campaigns. An overview of the laboratory and computational studies of the interference in different FAGE instruments is given in a recent review by Stone et al. (2012).

### 3.3 BBCEAS measurements of NO<sub>3</sub> and N<sub>2</sub>O<sub>5</sub>

NO<sub>3</sub> and N<sub>2</sub>O<sub>5</sub> were measured by the University of Cambridge broadband cavity enhanced absorption spectroscopy (BBCEAS) instrument. The instrument was designed and built specifically for the RONOCO project and is described in detail in Kennedy et al. (2011). A brief description is given here.

The instrument consists of three 94 cm long high finesse optical cavities formed by pairs of highly reflecting mirrors. The cavities are irradiated by incoherent broadband continuous wave light sources. Two of the cavities, for the detection of N<sub>2</sub>O<sub>5</sub> and NO<sub>3</sub>, are irradiated by red light emitting diodes (LEDs) centred at 660 nm. The third cavity, for the detection of NO<sub>2</sub>, is irradiated by a blue LED centred at 460 nm. The light from the LEDs is collimated using optical fibres and a focussing lens at the input of each cavity. A spectrometer, consisting of a spectrograph and charge couple device (CCD), is positioned at the end of each cavity to measure the wavelength-dependent intensity of transmitted light.

Ambient air is sampled through a rear-facing inlet on the aircraft fuselage, positioned approximately 4 m from the aircraft nose and 10 cm from the aircraft body. The air from the inlet is divided into two flows. The flow directed to the  $\text{N}_2\text{O}_5$  cavity is heated to 120 °C to ensure near complete ( $> 99.6\%$ ) thermal dissociation of  $\text{N}_2\text{O}_5$  to  $\text{NO}_2$  and  $\text{NO}_3$ . The cavity itself is heated to 80 °C and is used to measure the sum of the concentrations of ambient  $\text{NO}_3$  plus  $\text{NO}_3$  from thermal decomposition of  $\text{N}_2\text{O}_5$ . The second flow is unheated and is directed first through the  $\text{NO}_3$  cavity and then through the  $\text{NO}_2$  cavity. Background spectra are recorded at half hour intervals during flights by halting the flow of ambient air and purging the cavities with nitrogen.

$\text{NO}_3$  is detected by its strong  $\text{B}^2\text{E}' - \text{X}^2\text{A}'_2$  electronic transition centred at 662 nm. The concentration of  $\text{NO}_3$  is determined by separating the finely structured  $\text{NO}_3$  absorption features from the broad features caused by Rayleigh and Mie scattering using a fitting technique analogous to that employed in differential optical absorption spectroscopy (DOAS). A strong water vapour absorption feature that spectrally overlaps with  $\text{NO}_3$  absorption around 662 nm is simulated for the pressure and temperature measured in the cavity and is removed from the measured absorption spectrum. The concentration of  $\text{N}_2\text{O}_5$  is determined by subtracting the concentration of ambient  $\text{NO}_3$  measured in the unheated cavity from the sum of the concentrations of ambient and dissociated  $\text{NO}_3$  measured in the heated cavity.

Contributions to uncertainties in ambient measurements of  $\text{NO}_3$  and  $\text{N}_2\text{O}_5$ , including wall losses of  $\text{NO}_3$  and  $\text{N}_2\text{O}_5$ , temperature- and pressure-dependent absorption cross sections of  $\text{NO}_3$  and  $\text{H}_2\text{O}$ , and the length of the cavity occupied by the sample, have been thoroughly investigated in laboratory experiments or addressed in the data analysis routine. In addition, wall losses of  $\text{NO}_3$  and  $\text{N}_2\text{O}_5$  were determined before and after each flight to account for changes in the surface properties of the inlet and detection cell walls, which were found to be negligible. The total uncertainty in the measured concentration of ambient  $\text{NO}_3$  was 11 %. The uncertainty in the measured concentration of ambient  $\text{N}_2\text{O}_5$  is determined for each individual ambient measurement, being dependent on the  $\text{NO}_3/\text{N}_2\text{O}_5$  ratio, and was on the order of 15 %. During RONOCO flights the  $1\sigma$  limits of detection for  $\text{NO}_3$  and the sum of  $\text{NO}_3 + \text{N}_2\text{O}_5$  were 1.1 pptv and 2.4 pptv, respectively, for a 1 second integration time.

#### 4 Overview of OH and HO<sub>2</sub>\* measurements

FAGE measurements were made on 16 flights during RONOCO and 9 flights during SeptEx. There was insufficient laser power during flights B534 to B536 in the summer campaign to measure both OH and HO<sub>2</sub>\* by dividing the laser light between the two cells. OH was therefore not measured during these flights. Low laser power throughout the summer fieldwork caused relatively high fluctuations in laser power and therefore higher background variability. This resulted in higher limits of detection for OH ( $1.8 \times 10^6$  molecule cm<sup>-3</sup>) and HO<sub>2</sub>\* ( $6.9 \times 10^5$  molecule cm<sup>-3</sup>).

Table 4 summarises the OH and HO<sub>2</sub>\* measurements during RONOCO and SeptEx and gives the instrument's average 1 $\sigma$  limit of detection for a 5 minute averaging period. OH was not detected above the limit of detection during the summer or winter RONOCO flights, resulting in upper limits of  $1.8 \times 10^6$  molecule cm<sup>-3</sup> and  $6.4 \times 10^5$  molecule cm<sup>-3</sup> for mean summer and winter concentrations, respectively. These upper limit values are similar to previously reported nighttime OH measurements (Geyer et al., 2003; Holland et al., 2003; Ren et al., 2003b; Emmerson and Carslaw, 2009). The mean daytime OH concentration during SeptEx was  $1.8 \times 10^6$  molecule cm<sup>-3</sup>, which was above the limit of detection. The mean HO<sub>2</sub>\* mixing ratio was highest during SeptEx (2.9 pptv), and was higher during summer (1.6 pptv) than during winter (0.7 pptv). The OH and HO<sub>2</sub>\* datasets for RONOCO and SeptEx are shown as altitude profiles in Fig. 4 and Fig. 5, respectively.

Table 5 gives the mean and maximum HO<sub>2</sub>\* mixing ratios at different times of day during summer, SeptEx and winter. Dawn, day, dusk and night are defined by the solar zenith angle as follows: dawn and dusk are between 90 and 102° and are distinguished by the time of day; day is between 0° and 90°; night is between 102° and 180°.

The mean dusk HO<sub>2</sub>\* mixing ratio in summer was higher than the mean nighttime mixing ratio, suggesting that photochemical production was still active at dusk in summer. The reverse was true for the winter data, with the highest mean HO<sub>2</sub>\* mixing ratio being at night. This suggests that when photochemical production was suppressed in the winter daytime due to low photolysis rates, production via reactions of NO<sub>3</sub> and O<sub>3</sub> with alkenes was an important route to radical initiation. The RONOCO HO<sub>2</sub>\* measurements are similar to nighttime, ground-based, urban measurements. For example, during the TORCH campaign, [HO<sub>2</sub>] peaked at  $1 \times 10^8$  molecule cm<sup>-3</sup> at night (Emmerson et al., 2007), and during the

PMTACS-NY 2001 field campaign, nighttime HO<sub>2</sub> concentrations of  $8 \times 10^6$  molecule cm<sup>-3</sup> were measured (Ren et al., 2003b).

#### **4.1 Case study flight B537: high nighttime HO<sub>2</sub>\* concentrations**

The highest HO<sub>2</sub>\* concentration ( $3.2 \times 10^7$  molecule cm<sup>-3</sup>; 13.7 pptv) was measured during nighttime flight B537 on 20<sup>th</sup> July 2010. Take-off from East Midlands Airport was at 22:00 local time (21:00 UTC, sunset at 20:18 UTC). The flight track, coloured by altitude, is shown in Fig. 6. The flight involved a profile descent from 3350 m to 460 m down the Norfolk coast and a missed approach at Southend Airport (51.6° N, 0.70° E). Plumes from European continental outflow (see Fig. 7) were intersected by a series of runs at altitudes between 460 m and the upper boundary of the polluted layer.

Flight B537 is an unusual flight within the RONOCO dataset, with high concentrations of CO, O<sub>3</sub>, NO<sub>3</sub>, and high temperatures compared to the values measured during other nighttime flights (see Table 3). The ambient aerosol surface area was significantly higher during B537 (nearly 800 μm<sup>2</sup> cm<sup>-3</sup>) than during other flights (between 100 and 400 μm<sup>2</sup> cm<sup>-3</sup>), and the organic aerosol concentration was significantly enhanced (Morgan et al., 2014). Footprint maps for flight B537, indicating regions where the sampled air was in contact with the surface prior to the flight, are shown in Fig. 7. The air sampled during the flight originated primarily over northern France, Belgium and Germany.

A region of high surface pressure was positioned over the UK on the 20<sup>th</sup> July, with a mean air pressure of 1012.6 hPa over the 24 hours prior to the flight. The mean air temperature 24 hours prior to the flight (22:00 19/07/2010 to 22:00 20/07/2010), measured at a number of Met Office weather stations in Greater London, was 22.6 °C, and reached a maximum value of 28.6 °C. Wind speeds prior to the flight were low, with an average value of 4.7 knots (2.4 m s<sup>-1</sup>). No rainfall was recorded at any of the Greater London weather stations during the 24 hours prior to the flight. 12.4 hours of sunshine were recorded on the 20<sup>th</sup> July at Heathrow Airport (51.5 °N, 0.45 °W). High temperatures, combined with low wind speed, exposure to solar radiation, and little precipitation promote the formation of ozone as a result of photochemical processing of VOCs emitted at the surface (e.g. Lee et al., 2006), and offer an explanation for the high ozone mixing ratios measured during flight B537. Peak surface daytime ozone concentrations measured in Teddington, London, on 20<sup>th</sup> July were on the order of  $2.0 \times 10^{12}$  molecule cm<sup>-3</sup> (~78 ppbv) (data available at [www.airquality.co.uk](http://www.airquality.co.uk)). Similar levels were recorded at a number of locations within Greater London.

Figure 8 shows a time series of altitude, HO<sub>2</sub><sup>\*</sup>, O<sub>3</sub>, and NO<sub>3</sub> mixing ratios during the flight, demonstrating very similar behaviour between the two radical species. During the missed approach at Southend Airport the mixing ratios of HO<sub>2</sub><sup>\*</sup> and NO<sub>3</sub> increased with decreasing altitude, to reach values of 4.5 pptv and 35 pptv, respectively, at 50 m above the ground. The maximum HO<sub>2</sub><sup>\*</sup> and NO<sub>3</sub> mixing ratios were measured over the North Sea east of Ipswich (52.16 ° N, 2.34 ° E) at an altitude of 509 m, in the outflow of the London plume. Figure 9 shows scatter plots of HO<sub>2</sub><sup>\*</sup> against NO<sub>3</sub> and O<sub>3</sub> during flight B537 and during the other nighttime flights during RONOCO. Strong positive correlation is evident between HO<sub>2</sub><sup>\*</sup> and NO<sub>3</sub> during B537 ( $r = 0.97$ ), while during the remaining night flights there is still a significant, though weaker, correlation ( $r = 0.58$ ). Moderate negative correlation is evident between HO<sub>2</sub><sup>\*</sup> and O<sub>3</sub> during B537 ( $r = -0.46$ ), with weak positive correlation existing for the other nighttime flights ( $r = 0.19$ ). The data suggest that NO<sub>3</sub> was an important initiator of HO<sub>x</sub> radicals during flight B537, and that O<sub>3</sub> played a limited role overall during the nighttime flights. Further investigation of the roles of NO<sub>3</sub> and O<sub>3</sub> in alkene oxidation and radical initiation at night is described in Sect. 5.

## 5 Oxidation of alkenes and production of HO<sub>2</sub>: method of analysis

Following the work of Salisbury et al. (2001), the total rates of reaction,  $\Phi$ , of O<sub>3</sub> and NO<sub>3</sub> with the alkenes measured during RONOCO and SeptEx have been calculated:

$$\Phi_{O_3} = \sum_i^{\text{alkene}} k_{O_3+\text{alk}_i} [O_3][\text{alkene}_i] \quad (3)$$

$$\Phi_{NO_3} = \sum_i^{\text{alkene}} k_{NO_3+\text{alk}_i} [NO_3][\text{alkene}_i] \quad (4)$$

The reactions of O<sub>3</sub> and NO<sub>3</sub> with alkenes yield OH, HO<sub>2</sub>, and RO<sub>2</sub> radicals. Consideration of the reaction mechanisms of NO<sub>3</sub> and O<sub>3</sub> enables calculation of the rate of instantaneous production of HO<sub>2</sub> ( $P_{HO_2}$ ) from the reactions of NO<sub>3</sub> and O<sub>3</sub> with the alkenes measured during RONOCO, using the chemistry scheme, rate constants and branching ratios in the MCM (Jenkin et al., 1997; Saunders et al., 2003).

Figure 10 shows a generalized reaction scheme for the reaction of NO<sub>3</sub> with an alkene. The reaction between NO<sub>3</sub> and an alkene proceeds via addition of NO<sub>3</sub> to the double bond to form a nitrooxyalkyl radical, followed by rapid reaction with oxygen to yield a nitrooxyalkyl

peroxy radical, RO<sub>2</sub> (shown as a single step in Fig. 10). The RO<sub>2</sub> radical can react with a number of species, of which NO, NO<sub>3</sub> and RO<sub>2</sub> lead to production of an alkoxy radical (RO). Radical termination occurs via reaction of RO<sub>2</sub> with HO<sub>2</sub> to yield a peroxide (ROOH) or with RO<sub>2</sub> to yield carbonyl (RC(O)CH<sub>3</sub>) and alcohol (RCH<sub>2</sub>OH) products. Reaction of RO with oxygen proceeds via abstraction of a hydrogen atom to yield HO<sub>2</sub> or an aldehyde (RCHO). This generalised scheme can be applied to the reactions of NO<sub>3</sub> with all the alkenes measured. The rate of instantaneous production of HO<sub>2</sub> is found by first calculating the fraction of RO<sub>2</sub> that reacts to produce RO ( $F_{RO}$ ), and the fraction of RO that reacts to produce HO<sub>2</sub> ( $F_{HO_2}$ ):

$$F_{RO} = \frac{k_3[NO] + k_4[NO_3] + 0.6k_5[RO_2]}{k_2[HO_2] + k_3[NO] + k_4[NO_3] + k_5[RO_2]} \quad (5)$$

$$F_{HO_2} = \frac{k_6[O_2]}{k_7 + k_6[O_2]} \quad (6)$$

where RO<sub>2</sub> represents all peroxy radicals. Average values of  $F_{RO}$  for the NO<sub>3</sub> + alkene reactions range between 0.50 for *trans*-2-pentene- and 1-pentene-derived RO<sub>2</sub> species and 0.61 for ethene-derived RO<sub>2</sub> species.  $F_{HO_2}$  varies between 0 and 1 for the alkenes studied. Overall, the rate of production of HO<sub>2</sub> ( $P_{HO_2}$ ) from reactions of NO<sub>3</sub> with alkenes is then given by:

$$P_{HO_2} = k_i[NO_3][alkene_i] \times F_{RO} \times F_{HO_2} \quad (7)$$

The reaction scheme for the reaction of O<sub>3</sub> with alkenes is more complicated because the number and type of radicals produced in the O<sub>3</sub> + alkene reaction depends on the structure of the alkene. The simplest case is the reaction of ozone with ethene. Ozone adds to the double bond to form a five-membered ring called a primary ozonide. Decomposition of the ozonide yields an excited Criegee intermediate (CH<sub>2</sub>OO<sup>\*</sup>) and a carbonyl compound (in this case formaldehyde, HCHO). The energy-rich Criegee intermediate can be stabilised by collision with a third body or undergo decomposition to yield products including OH, CO, and HO<sub>2</sub>. The primary ozonide produced in the O<sub>3</sub> + propene reaction (see Fig. 11) can decompose via two channels, yielding carbonyls and Criegee intermediates with different structures and different products, including RO<sub>2</sub>. Reaction of RO<sub>2</sub> with NO, NO<sub>3</sub> and RO<sub>2</sub> (all peroxy radicals) yields RO, which in turn yields HO<sub>2</sub>.

493 The rates of production of HO<sub>2</sub> from reactions of O<sub>3</sub> with alkenes ( $P_{\text{HO}_2}$ ) have been  
 494 calculated as follows:

$$495 \quad P_{\text{HO}_2, \text{Direct}} = k_i [\text{O}_3] [\text{alkene}_i] \times \alpha_{\text{HO}_2} \quad (8)$$

$$496 \quad P_{\text{HO}_2, \text{RO}_2} = k_i [\text{O}_3] [\text{alkene}_i] \times \alpha_{\text{RO}_2} \times F_{\text{RO}} \times F_{\text{HO}_2} \quad (9)$$

$$497 \quad P_{\text{HO}_2} = P_{\text{HO}_2, \text{Direct}} + P_{\text{HO}_2, \text{RO}_2} \quad (10)$$

498 where  $P_{\text{HO}_2, \text{Direct}}$  is the rate of direct HO<sub>2</sub> production from Criegee intermediate  
 499 decomposition,  $\alpha_{\text{HO}_2}$  is the branching ratio to HO<sub>2</sub>-producing channels from the Criegee  
 500 intermediate,  $P_{\text{HO}_2, \text{RO}_2}$  is the rate of HO<sub>2</sub> production from RO<sub>2</sub> radicals produced in the O<sub>3</sub> +  
 501 alkene reaction,  $\alpha_{\text{RO}_2}$  is the branching ratio to RO<sub>2</sub>-producing channels from the Criegee  
 502 intermediate,  $F_{\text{RO}}$  is the fraction of RO<sub>2</sub> radicals that react to produce RO radicals, and  $F_{\text{HO}_2}$   
 503 is the fraction of RO radicals that react to produce HO<sub>2</sub> radicals, which is equal to 1 for all the  
 504 alkenes studied. Average values of  $F_{\text{RO}}$  for the O<sub>3</sub> + alkene reactions range between 0.54 for  
 505 1-pentene-derived RO<sub>2</sub> species and 0.64 for 1-butene- and *trans*-2-pentene-derived RO<sub>2</sub>  
 506 species.

507 The reactions of RO<sub>2</sub> with NO to form RONO<sub>2</sub> have been omitted from the calculations  
 508 because the branching ratio is small (0.001 to 0.02) for the radicals studied (Carter and  
 509 Atkinson, 1989; Lightfoot et al., 1992). The reaction of CH<sub>3</sub>O<sub>2</sub> with NO<sub>2</sub> to form CH<sub>3</sub>O<sub>2</sub>NO<sub>2</sub>  
 510 has been omitted from the calculations, since the reverse reaction is much faster than the  
 511 forward direction ( $k_f = 6.4 \times 10^{-12} \text{ s}^{-1}$ ;  $k_{\text{rev}} = 1.08 \text{ s}^{-1}$  at a mean temperature of 286.5 K during  
 512 RONOCO).

513 The primary aims of the analysis presented here are threefold: 1. To calculate the total rate of  
 514 initiation through reactions of NO<sub>3</sub> and O<sub>3</sub> with alkenes; 2. To determine the relative  
 515 importance of NO<sub>3</sub> and O<sub>3</sub> in nighttime HO<sub>2</sub> production; 3. To investigate differences in  
 516 radical production between different seasons and different times of day. The correlation  
 517 between [HO<sub>2</sub>\*] and [NO<sub>3</sub>], especially during flight B537, will be investigated.

518  $P_{\text{HO}_2}$  has been calculated for each alkene measured for every 60-second data point where all  
 519 the requisite data were available and where HO<sub>2</sub>\* was above the limit of detection of the  
 520 FAGE instrument. Concentrations of RO<sub>2</sub> were calculated by scaling the observed HO<sub>2</sub>\*  
 521 concentrations with the RO<sub>2</sub>/HO<sub>2</sub>\* ratio calculated using a box model constrained to the



concentrations of long-lived species measured during the flights (Stone et al., 2014b), i.e.  $RO_{2,obs} = HO_2^*_{,obs} \times RO_{2,mod}/HO_2^*_{,mod}$ . The rates of reaction and rates of production of  $HO_2$  presented hereafter are average values for individual flights, seasons, or times of day.

## 6 Results

### 6.1 Nighttime oxidation of alkenes

Figure 12 shows histograms of the rate of reaction between  $O_3$  and  $NO_3$  with individual alkenes during summer and winter, for the nighttime data only. The reactivity of measured alkenes ( $\Phi_{O_3} + \Phi_{NO_3}$ ) was greater during summer flights than during winter flights by a factor of 2.2. The reactions of  $NO_3$  are largely responsible for this seasonal difference, since the contribution from  $O_3$  + alkene reactions varies little between summer ( $4.1 \times 10^4$  molecule  $cm^{-3} s^{-1}$ ) and winter ( $3.9 \times 10^4$  molecule  $cm^{-3} s^{-1}$ ). The factor of 4.1 difference between the rate of  $NO_3$  reactions in summer ( $9.8 \times 10^4$  molecule  $cm^{-3} s^{-1}$ ) and winter ( $2.4 \times 10^4$  molecule  $cm^{-3} s^{-1}$ ) can be attributed to the higher mean concentration of  $NO_3$  in summer ( $5.8 \times 10^8$  molecule  $cm^{-3}$ ) compared to winter ( $2.0 \times 10^8$  molecule  $cm^{-3}$ ). This seasonal difference in  $NO_3$  concentrations is attributable to the lower mean nighttime temperature in winter (277.7 K) compared to summer (286.7 K) which disfavors  $NO_3$  in the thermal equilibrium  $N_2O_5 \rightleftharpoons NO_3 + NO_2$ .  $K_{eq}[NO_2]$ , which determines  $[N_2O_5]/[NO_3]$ , is calculated to be 4.8 in summer and 29.6 in winter. At night in summer,  $\Phi_{NO_3}$  was greater than  $\Phi_{O_3}$  by a factor of 2.4, but in winter  $\Phi_{O_3}$  was a factor of 1.6 greater than  $\Phi_{NO_3}$ . Figure 12 illustrates the importance of the butene isomers (within the VOCs measured) in the reactions of  $O_3$  and  $NO_3$ , and therefore radical initiation and propagation. Reactions with *iso*-butene dominated  $NO_3$  reactivity in summer (42 %) and winter (53 %), with *trans*-2-butene also contributing significantly (28 % in summer and 32 % in winter). Reactions of  $O_3$  were dominated by *trans*-2-butene (42 % in summer and 34 % in winter) and propene (26 % in summer and 38 % in winter). The importance of these alkenes is attributed to their relatively high abundances compared to the other alkenes measured, during both summer and winter, combined with their fast rates of reaction with  $O_3$  and  $NO_3$ .

For comparison with the reactions of  $O_3$  and  $NO_3$ , the total rate of reaction of measured alkenes with OH has been calculated using upper limits on OH concentrations of  $1.8 \times 10^6$  molecule  $cm^{-3}$  and  $6.4 \times 10^5$  molecule  $cm^{-3}$  for the summer and winter flights, respectively, based on the FAGE instrument's limit of detection. The high upper limits make the total rate

of reaction of OH with alkenes,  $\Phi_{\text{OH}}$ , unrealistically high for both summer ( $1.6 \times 10^5$  molecule  $\text{cm}^{-3} \text{s}^{-1}$ ) and winter ( $7.8 \times 10^4$  molecule  $\text{cm}^{-3} \text{s}^{-1}$ ). However, the OH reactivity will likely be considerably lower than the values calculated using the OH upper limits. A box model constrained to concentrations of long-lived species measured during the flights (Stone et al., 2014b) predicts a mean OH concentration of  $2.4 \times 10^4$  molecule  $\text{cm}^{-3}$ , significantly lower than the upper limits given by the instrument's limit of detection. Using the mean modelled value for OH gives  $\Phi_{\text{OH}} = 2.1 \times 10^3$  molecule  $\text{cm}^{-3} \text{s}^{-1}$  for summer, and  $\Phi_{\text{OH}} = 2.9 \times 10^3$  molecule  $\text{cm}^{-3} \text{s}^{-1}$  for winter, indicating a diminished role for OH in alkene oxidation at night in agreement with previous studies (e.g. Geyer et al., 2003; Emmerson et al., 2005).

## 6.2 Daytime oxidation of alkenes

Figure 13 shows histograms of rates of reaction of  $\text{O}_3$  and OH with alkenes during SeptEx, and  $\text{O}_3$  and  $\text{NO}_3$  with alkenes during winter RONOCO flights, for daytime data only. OH was detected above the limit of detection ( $1.2 \times 10^6$  molecule  $\text{cm}^{-3}$ ) during the SeptEx flights, so the FAGE OH data were included in the calculations, using a reaction scheme analogous to the one shown in Fig. 10.  $\text{NO}_3$  was not detected during the day in SeptEx.  $\text{NO}_3$  is not expected to be present at measurable concentrations during daylight hours due to photolysis, but a mean concentration of  $8.3 \times 10^7$  molecule  $\text{cm}^{-3}$  (3.3 pptv) was measured during the day in the winter RONOCO flights. These measurements of low mixing ratios of  $\text{NO}_3$  may be partly caused by interference from other daytime species as observed by Brown et al. (2005), or by the variability of the instrument baseline, which can be on the order of 1–2 pptv during vertical profiles on the aircraft (Kennedy et al., 2011). This variability is small compared to the range of  $\text{NO}_3$  values typically observed during RONOCO flights (0–50 pptv during summer; 0–10 pptv during winter). During SeptEx,  $\Phi_{\text{OH}}$  exceeded  $\Phi_{\text{O}_3}$  by a factor of 8. Ethene and propene were the two most abundant alkenes measured during SeptEx and contributed significantly to OH reactivity.  $\text{O}_3$  reactivity with alkenes was dominated by propene and *trans*-2-butene (6<sup>th</sup> most abundant alkene measured during SeptEx).  $\text{NO}_3$  reactivity with alkenes was dominated by *trans*-2-butene and isobutene (3<sup>rd</sup> most abundant alkene measured during winter daytime flights). The total rate of reaction of  $\text{O}_3$  and OH with alkenes during daytime SeptEx flights ( $3.7 \times 10^5$  molecule  $\text{cm}^{-3} \text{s}^{-1}$ ) exceeded the total rate of reaction of  $\text{O}_3$  and  $\text{NO}_3$  during daytime winter RONOCO flights ( $6.6 \times 10^4$  molecule  $\text{cm}^{-3} \text{s}^{-1}$ ) by a factor of 6, and was more than double the total rate of reaction of  $\text{O}_3$  and  $\text{NO}_3$  with

alkenes during nighttime summer flights ( $1.4 \times 10^5$  molecule  $\text{cm}^{-3} \text{s}^{-1}$ ). In winter daytime flights,  $\Phi_{\text{O}_3}$  was greater than  $\Phi_{\text{NO}_3}$  by a factor of 2.4.

Figure 12b and Fig. 13b reveal that reactions of  $\text{O}_3$  dominated alkene reactivity during both daytime and nighttime winter RONOCO flights. The concentrations of alkenes were generally higher at night, with the total alkene concentration (sum of concentrations of alkenes measured) being  $2.1 \times 10^9$  molecule  $\text{cm}^{-3}$  in the day, and  $3.4 \times 10^9$  molecule  $\text{cm}^{-3}$  at night. The total measured alkene reactivity ( $\Phi_{\text{O}_3} + \Phi_{\text{NO}_3}$ ) was marginally higher during the day, by a factor of 1.04. This difference is attributable mainly to the change in  $\Phi_{\text{O}_3}$ .

Comparison of Fig. 12a and Fig. 13b reveals that the total measured alkene reactivity ( $\Phi_{\text{O}_3} + \Phi_{\text{NO}_3}$ ) was higher during the summer nighttime flights ( $1.4 \times 10^5$  molecule  $\text{cm}^{-3} \text{s}^{-1}$ ) than during the winter daytime flights ( $6.6 \times 10^4$  molecule  $\text{cm}^{-3} \text{s}^{-1}$ ), indicating a low oxidising environment during winter daytime. The additional contribution to measured alkene reactivity from reactions with OH has been calculated using the OH upper limits as described in Sect. 6.1. Even with this additional, upper limit OH reactivity ( $1.6 \times 10^5$  molecule  $\text{cm}^{-3} \text{s}^{-1}$  and  $1.1 \times 10^5$  molecule  $\text{cm}^{-3} \text{s}^{-1}$  for summer nighttime and winter daytime, respectively) the total summer nighttime alkene reactivity remains higher than that during winter daytime, confirming the importance of the summer nocturnal troposphere for the oxidation of the measured alkenes.

### 6.3 Nighttime production of $\text{HO}_2$ from reactions of $\text{O}_3$ and $\text{NO}_3$ with alkenes

Table 6 gives total rates ( $\Sigma P_{\text{HO}_2}$ ) of instantaneous production of  $\text{HO}_2$  from the reactions of  $\text{O}_3$  and  $\text{NO}_3$  with alkenes.  $\text{NO}_3$  was not detected during the dawn summer RONOCO flights and there were no daytime RONOCO flights during summer.  $\text{NO}_3$  dominated  $\text{HO}_2$  production during dusk and night (68 %), in agreement with Geyer et al. (2003) who found that  $\text{NO}_3$  was responsible for 53 % of  $\text{HO}_2$  production at night in the BERLIOZ campaign. During winter,  $\text{O}_3$  dominated  $\text{HO}_2$  production at all times, with a nighttime contribution of 70 %. This is in agreement with the results from the winter PMTACS-NY 2004 field campaign (Ren et al., 2006).

The total rate of instantaneous production of  $\text{HO}_2$  at night was 3.3 times greater in summer than in winter, with production from  $\text{O}_3$  decreasing by a factor of 1.5, and production from  $\text{NO}_3$  decreasing by a factor of 7.8, between summer and winter. The mean temperature difference between summer and winter of 9 K is thought to be responsible for the lower  $\text{NO}_3$  concentrations in winter ( $2.0 \times 10^8$  molecule  $\text{cm}^{-3}$ , 8.2 pptv, compared to  $5.8 \times 10^8$  molecule

cm<sup>-3</sup>, 24.5 pptv in summer), owing to the increased thermal stability of N<sub>2</sub>O<sub>5</sub>, and for the reduced rate of temperature-dependent reactions between NO<sub>3</sub> and alkenes, and subsequent reactions. There was very little difference between summer and winter mean O<sub>3</sub> mixing concentrations ( $9.6 \times 10^{11}$  molecule cm<sup>-3</sup>, 39.6 ppbv, and  $9.4 \times 10^{11}$  molecule cm<sup>-3</sup>, 38.6 ppbv, respectively).

Production of HO<sub>2</sub> via reactions of NO<sub>3</sub> and O<sub>3</sub> with alkenes is now examined in more detail. The rate of production from individual alkenes was calculated, and plotted in a histogram, as shown in Fig. 14 for the summer and winter nighttime data. During both summer and winter, reactions of O<sub>3</sub> and NO<sub>3</sub> with *trans*-2-butene were important sources of HO<sub>2</sub>, contributing on average 62 % to O<sub>3</sub>-initiated HO<sub>2</sub> production and 36 % to NO<sub>3</sub>-initiated production during the summer and winter flights. Reactions of NO<sub>3</sub> with isoprene were important during summer, contributing 28 % to NO<sub>3</sub>-initiated production. The importance of *trans*-2-butene, despite its relatively low abundance during summer and winter nighttime RONOCO flights (1.8 pptv and 1.7 pptv, respectively, compared to ethene mixing ratios of 55.0 and 104.5 pptv), is attributed to its fast rates of reaction with both O<sub>3</sub> and NO<sub>3</sub> compared to the other alkenes measured. The importance of the isoprene + NO<sub>3</sub> reactions during the summer RONOCO flights is similarly attributed to its fast rate of reaction with NO<sub>3</sub> compared to the other alkenes measured. In addition there is no aldehyde-forming channel from the isoprene-derived RO radical ( $k_7$  in Fig. 10), so that the yield of HO<sub>2</sub> from RO is equal to 1. The reaction of isobutene with NO<sub>3</sub> can proceed via one of two channels to produce two different RO<sub>2</sub> radicals but only one channel, with a branching ratio of 0.2, produces HO<sub>2</sub>. Isobutene is therefore not a dominant contributor to HO<sub>2</sub> production, despite being the single largest contributor to NO<sub>3</sub> reactivity during daytime and nighttime RONOCO flights (Fig. 12 and Fig. 13). Figure 14 highlights the small change in total production from O<sub>3</sub> between summer and winter, and the dramatic change in total production from NO<sub>3</sub> between summer and winter.

Reactions of formaldehyde with NO<sub>3</sub> were included in the analysis where formaldehyde data were available (mean HCHO = 955 pptv). The NO<sub>3</sub> + HCHO reaction contributed a further  $5.5 \times 10^3$  molecule cm<sup>-3</sup> s<sup>-1</sup> (15 %) to HO<sub>2</sub> production from NO<sub>3</sub> reactions, so that production from NO<sub>3</sub> contributed 79 % of the total production.

## 6.4 Production of HO<sub>2</sub> during flight B537

Flight B537, on 20<sup>th</sup> July 2010, has been identified as an interesting flight, with high concentrations of HO<sub>2</sub>\* ( $3.2 \times 10^8$  molecule cm<sup>-3</sup>; 13.6 pptv), ozone (peaking at  $1.8 \times 10^{12}$  molecule cm<sup>-3</sup>, 89.9 ppbv) and NO<sub>3</sub> (peaking at  $4.1 \times 10^9$  molecule cm<sup>-3</sup>; 176.9 pptv), and a strong positive correlation between HO<sub>2</sub>\* and NO<sub>3</sub> ( $r = 0.97$ , see Fig. 9). NO, NO<sub>2</sub>, and aerosol surface area were also elevated during the flight during flight B537 compared to their mean summer values. The highest concentration of ethene ( $1.43 \times 10^{10}$  molecule cm<sup>-3</sup>; 0.61 ppbv) during the summer RONOCO flights was measured during B537.  $\Sigma P_{\text{HO}_2}$  from O<sub>3</sub> + alkene reactions ( $2.6 \times 10^4$  molecule cm<sup>-3</sup> s<sup>-1</sup>) was higher in flight B537 than in all the other summer flights, contributing 42 % of HO<sub>2</sub> production, with NO<sub>3</sub> + alkene reactions contributing  $3.6 \times 10^4$  molecule cm<sup>-3</sup> (58 %). The total rate of HO<sub>2</sub> production from O<sub>3</sub> and NO<sub>3</sub> reactions during flight B537 was  $6.2 \times 10^4$  molecule cm<sup>-3</sup> s<sup>-1</sup>. While this is higher than the average value of  $\Sigma P_{\text{HO}_2}$  for the summer flights ( $5.4 \times 10^4$  molecule cm<sup>-3</sup> s<sup>-1</sup>) it is not the highest rate of production during the summer flights. During B534 unusually high concentrations of isoprene, *cis*-2-butene, and 1,3-butadiene contributed to a total rate of HO<sub>2</sub> production of  $7.9 \times 10^4$  molecule cm<sup>-3</sup>, which is the highest calculated value.

Figure 15 shows that the reactions of O<sub>3</sub> and NO<sub>3</sub> with *trans*-2-butene are once again important, contributing 74 % of  $\Sigma P_{\text{HO}_2, \text{O}_3}$ , and 45 % of  $\Sigma P_{\text{HO}_2, \text{NO}_3}$ . The correlation between HO<sub>2</sub>\* and NO<sub>3</sub> is attributed to production of HO<sub>2</sub> by reactions of NO<sub>3</sub> with alkenes, especially *trans*-2-butene. Figure 16 shows HO<sub>2</sub>\* versus the total instantaneous rate of production from the reactions of O<sub>3</sub> and NO<sub>3</sub> with alkenes during flight B537, at each 60-second data point during the flight for which the requisite data were available. Note that the rates plotted in Fig. 16 are higher than those shown in Fig. 15, where the rates of production of HO<sub>2</sub> from each alkene have been averaged across the whole flight. A strong positive correlation exists between HO<sub>2</sub>\* and both  $\Sigma P_{\text{HO}_2, \text{O}_3}$  ( $r = 0.6$ ) and  $\Sigma P_{\text{HO}_2, \text{NO}_3}$  ( $r = 0.8$ ), indicating the importance of these reactions for production of HO<sub>2</sub> during this flight.

## 7 Comparison with model results

The observations of OH, HO<sub>2</sub>\*, NO<sub>3</sub> and N<sub>2</sub>O<sub>5</sub> have been interpreted in the context of nighttime oxidation chemistry using a box model constrained to observations of VOCs, NO<sub>x</sub>, O<sub>3</sub>, CO and other long-lived species measured during the RONOCO flights (Stone et al., 2014b). The Dynamically Simple Model of Atmospheric Chemical Complexity (DSMACC)

(Emmerson and Evans, 2009; Stone et al., 2010; Stone et al., 2014b) was initiated with concentrations of measured species, using a chemistry scheme based on the Master Chemical Mechanism (MCM, version 3.2: Jenkin et al., 1997; Jenkin et al., 2003; Saunders et al., 2003; Bloss et al., 2005, via <http://mcm.leeds.ac.uk/MCM>) and was allowed to run to diurnal steady state. The model output includes concentrations of OH, HO<sub>2</sub>, NO<sub>3</sub>, RO<sub>2</sub>, and other species. Data from daytime flights, or during dawn or dusk periods, were not included in the model analysis. Data from flight B537 were also excluded, owing to the atypical observations of HO<sub>2</sub>\*, NO<sub>3</sub>, O<sub>3</sub> and other chemical species made during this flight. The modelling study and results are described in more detail by Stone et al. (2014b).

The model predicts a mean OH concentration of  $2.4 \times 10^4$  molecule cm<sup>-3</sup> for the summer flights, which is consistent with the measured OH concentrations for which the instrument's limit of detection is an upper limit only. The base model underpredicts HO<sub>2</sub>\* by around 200 %, and overpredicts NO<sub>3</sub> and N<sub>2</sub>O<sub>5</sub> by 80 and 50 %, respectively. These discrepancies were investigated by determining the processes controlling radical production and loss in the model, and using those results to improve model performance. Model production of HO<sub>2</sub> is dominated by reactions of RO + O<sub>2</sub> (42 %), with a significant contribution from OH + CO (31 %) despite low OH concentrations at night. RO<sub>x</sub> (= RO + RO<sub>2</sub> + OH + HO<sub>2</sub>) radical initiation in the model is dominated by reactions of NO<sub>3</sub> with unsaturated VOCs (80 %), with a much smaller contribution (18 %) from alkene ozonolysis. Modelled HO<sub>2</sub> loss is dominated by its reactions with NO<sub>3</sub> (45 %) and O<sub>3</sub> (27 %), both of which are radical propagating routes, and which are the dominant routes to OH production in the model. In fact NO<sub>3</sub> was found to control both radical initiation and propagation in the model.

These results are in general agreement with the results of the analysis presented in Sect. 6.1, though the model predicts a more important role for NO<sub>3</sub> (80 % of RO<sub>x</sub> radical production, which is 7.2 times the contribution from O<sub>3</sub> + alkenes) than is predicted by the analysis based on the observations alone (69 % of HO<sub>2</sub> radical production during summer, which is 2.1 times the contribution from O<sub>3</sub> + alkenes). The model predicts a relatively small role for O<sub>3</sub> in both summer and winter. The model is constrained to measured values of O<sub>3</sub>, but overpredicts NO<sub>3</sub>. The mean measured NO<sub>3</sub> nighttime mixing ratio was 24.5 pptv in the summer and 8.2 pptv in the winter. The mean modelled summer and winter values are 37.4 pptv and 20.7 pptv, respectively. This discrepancy between modelled and measured NO<sub>3</sub> helps to explain the model overprediction of the role of NO<sub>3</sub> in HO<sub>x</sub> radical initiation during the RONOCO flights. Modelled NO<sub>3</sub> reactivity was dominated by *iso*-butene (36 %) and *trans*-

2-butene (27 %), and modelled O<sub>3</sub> reactivity was dominated by *trans*-2-butene (51 %), in agreement with the nighttime alkene reactivities presented in Sect. 6.1.

Improvement to the model predictions of NO<sub>3</sub>, N<sub>2</sub>O<sub>5</sub> and HO<sub>2</sub>\* was made by increasing the concentration of unsaturated VOCs in the model. Increasing the total observed alkene concentration by 4 times resulted in a modelled to observed ratio of 1.0 for HO<sub>2</sub>\* and of ~1.2 for NO<sub>3</sub> and N<sub>2</sub>O<sub>5</sub>. Two-dimensional gas chromatography (GC × GC) analysis of the whole air samples taken during RONOCO has revealed a large number of VOCs extra to those routinely measured (Lidster et al., 2014). Calibration standards for the majority of these species are not yet available, and so quantification of their concentrations is not possible, but their detection confirms that the model overprediction of NO<sub>3</sub> and underprediction of HO<sub>2</sub>\* are attributable to reactions of NO<sub>3</sub> with unquantified unsaturated hydrocarbons.

The presence of unquantified unsaturated VOCs during the RONOCO campaign, suggested by the model and confirmed by the two-dimensional GC analysis, has implications for the conclusions drawn from the analysis based on the observations. The relative contributions of NO<sub>3</sub> and O<sub>3</sub> to nighttime radical initiation will change with the composition of unsaturated VOCs in the sampled air, due to the different rates of reaction of NO<sub>3</sub> and O<sub>3</sub> with different VOC species, and the rates of production of HO<sub>2</sub> following these reactions. The model results indicate that reaction of NO<sub>3</sub> with the unquantified VOCs leads to increased production of HO<sub>2</sub>. The role of NO<sub>3</sub> in nighttime radical production would therefore be enhanced by the inclusion of the unquantified VOCs in the observational analysis.

## 8 Conclusions and future work

Nighttime radical chemistry has been studied as part of the RONOCO and SeptEx campaigns onboard the BAe-146 research aircraft during summer 2010 and winter 2011. NO<sub>3</sub>, N<sub>2</sub>O<sub>5</sub>, OH and HO<sub>2</sub>\* were measured simultaneously for the first time from an aircraft, with OH and HO<sub>2</sub>\* being measured by the University of Leeds aircraft FAGE instrument. OH was detected above the limit of detection during the daytime SeptEx flights only, with a mean concentration of  $1.8 \times 10^6$  molecule cm<sup>-3</sup>. Upper limits of  $1.8 \times 10^6$  molecule cm<sup>-3</sup> and  $6.4 \times 10^5$  molecule cm<sup>-3</sup> are placed on mean OH concentrations for the summer and winter RONOCO (night, dawn, and dusk) measurement campaigns, respectively. HO<sub>2</sub>\* was detected above the limit of detection during the summer and winter RONOCO flights and during SeptEx, with a maximum mixing ratio of 13.6 pptv measured during nighttime flight B537 on

20<sup>th</sup> July 2010. Mean nighttime HO<sub>2</sub>\* mixing ratios were significantly higher in summer than in winter. Significant concentrations (up to 176.9 pptv) of NO<sub>3</sub> were measured during nighttime flights, since the air masses sampled were sufficiently removed from the surface that the loss of NO<sub>3</sub> by reaction with NO was minimised. The RONOCO flights were therefore an excellent opportunity to study the role of NO<sub>3</sub> in nocturnal oxidation and radical initiation.

The rates of reaction of O<sub>3</sub> and NO<sub>3</sub> with the alkenes measured have been calculated. At night during summer, NO<sub>3</sub> dominated alkene reactivity. Several previous nighttime studies have also found NO<sub>3</sub> to be the dominant nocturnal oxidant (e.g. Geyer et al., 2003; Brown et al., 2011). During nighttime winter RONOCO flights the total rate of reaction of NO<sub>3</sub> with alkenes was much reduced, but the rate of reaction of O<sub>3</sub> with alkenes was similar to that in summer. During day and night in winter, O<sub>3</sub> + alkene reactions were faster than NO<sub>3</sub> + alkene reactions. Overall, during RONOCO, the combined rate of alkene oxidation by O<sub>3</sub> and NO<sub>3</sub> was highest at night during summer.

Calculation of rates of instantaneous production of HO<sub>2</sub> from reactions of O<sub>3</sub> and NO<sub>3</sub> with alkenes, using measurements made during the flights, has revealed that nighttime production was dominated by NO<sub>3</sub> in summer and by O<sub>3</sub> in winter. The rate of instantaneous production of HO<sub>2</sub> from reactions of NO<sub>3</sub> with alkenes decreased significantly from summer to winter (87 %), whereas production from O<sub>3</sub> + alkene reactions was similar in summer and winter, decreasing by just 31 %. Strong positive correlation between HO<sub>2</sub>\* and NO<sub>3</sub>, especially during flight B537, is attributed to the production of HO<sub>2</sub> from reactions of NO<sub>3</sub> with alkenes, particularly *trans*-2-butene and other isomers of butene.

Significant concentrations of HO<sub>2</sub>\* were detected at night, with the highest HO<sub>2</sub>\* concentration (13.6 pptv) being measured during a summer nighttime flight, indicating that HO<sub>x</sub> radical chemistry remains active at night under the right conditions. The role of HO<sub>x</sub> is diminished in the low photolysis winter daytime atmosphere, with alkene ozonolysis being primarily responsible for oxidation and radical initiation, in agreement with previous studies (e.g. Heard et al., 2004; Emmerson et al., 2005). Both the analysis presented here and the results of the box modelling study by Stone et al. (2014b) indicate that in air masses removed from sources of NO, NO<sub>3</sub> plays an important role in the oxidation of alkenes and radical initiation at night, in agreement with previous studies (e.g. Brown et al., 2011). Alkene ozonolysis also plays a significant role in nocturnal oxidation in agreement with Salisbury et al. (2001), Geyer et al. (2003), Ren et al. (2003a), Emmerson et al. (2005), Ren et al. (2006),



and Volkamer et al. (2010). The balance between the roles of  $\text{NO}_3$  and  $\text{O}_3$  was controlled in part by  $[\text{NO}_3]$ , with colder winter temperatures forcing the  $\text{NO}_3\text{--N}_2\text{O}_5$  equilibrium towards  $\text{N}_2\text{O}_5$ .

The total rate of reaction of  $\text{O}_3$  and  $\text{NO}_3$  with alkenes during nighttime summer flights ( $1.4 \times 10^5 \text{ molecule cm}^{-3} \text{ s}^{-1}$ ) was higher than during daytime winter flights ( $6.6 \times 10^4 \text{ molecule cm}^{-3} \text{ s}^{-1}$ ) by a factor of 2.1. Whilst it should be remembered that measurements at different times of day and in different seasons reflect composition changes in air masses (such as the abundance of reactive alkenes) this result supports the hypothesis that oxidation of certain VOCs, in particular the reactive alkenes, in the nocturnal summer atmosphere can be as rapid as in the winter daytime atmosphere.

A box model of nighttime chemistry constrained to measurements of long lived species has been used to investigate the nighttime chemistry sampled during RONOCO (Stone et al., 2014b). The base model underpredicts  $\text{HO}_2^*$  and overpredicts  $\text{NO}_3$ . These discrepancies were minimised by increasing the concentration of alkenes in the model, thereby increasing reaction of  $\text{NO}_3$  with alkenes, and production of  $\text{HO}_2$ . The presence of unquantified unsaturated VOCs has been confirmed by 2D-GC analysis, though the exact nature and concentrations of the ‘missing’ species is unclear. The inclusion of these species in the analysis presented in this paper would likely increase the role of  $\text{NO}_3$  for oxidation of alkenes and production of  $\text{HO}_2$  at night.

## Acknowledgements

This work was funded by the UK Natural Environment Research Council (NE/F004664/1). The authors would like to thank ground staff, engineers, scientists and pilots involved in RONOCO for making this project a success. Airborne data were obtained using the BAe 146-301 Atmospheric Research Aircraft (ARA) flown by Directflight Ltd. and managed by the Facility for Airborne Atmospheric Measurements (FAAM), which is a joint entity of the Natural Environment Research Council (NERC) and the Met Office.

## References

- Andrés-Hernández, M. D., Kartal, D., Crowley, J. N., Sinha, V., Regelin, E., Martínez-  
Harder, M., Nenakhov, V., Williams, J., Harder, H., Bozem, H., Song, W., Thieser, J., Tang,  
M. J., Hosaynali Beigi, Z., and Burrows, J. P.: Diel peroxy radicals in a semi-industrial  
coastal area: nighttime formation of free radicals, *Atmospheric Chemistry and Physics*, 13,  
5731-5749, 2013.
- Atkinson, R., and Arey, J.: Gas-phase tropospheric chemistry of biogenic volatile organic  
compounds: a review, *Atmospheric Environment*, 37, 197-219, 2003.
- Beames, J. M., Liu, F., Lu, L., and Lester, M. I.: Ultraviolet Spectrum and Photochemistry of  
the Simplest Criegee Intermediate  $\text{CH}_2\text{OO}$ , *Journal of the American Chemical Society*, 134,  
20045-20048, 2012.
- Beames, J. M., Liu, F., Lu, L., and Lester, M. I.: UV spectroscopic characterization of an  
alkyl substituted Criegee intermediate  $\text{CH}_3\text{CHOO}$ , *Journal of Chemical Physics*, 138, 244307,  
doi:10.1063/1.4810865, 2013.
- Berndt, T., and Böge, O.: Kinetics of Oxirane Formation in the Reaction of Nitrate Radicals  
with Tetramethylethylene, *Berichte der Bunsengesellschaft für physikalische Chemie*, 98,  
869-871, 1994.
- Bey, I., Aumont, B., and Toupance, G.: A modeling study of the nighttime radical chemistry  
in the lower continental troposphere, *Journal of Geophysical Research: Atmospheres*, 106,  
9991-10001, 2001.
- Bloss, C., Wagner, V., Bonzanini, A., Jenkin, M. E., Wirtz, K., Martin-Reviejo, M., and  
Pilling, M. J.: Evaluation of detailed aromatic mechanisms (MCMv3 and MCMv3.1) against  
environmental chamber data, *Atmospheric Chemistry and Physics*, 5, 623-639, 2005.
- Brown, S. S., and Stutz, J.: Nighttime radical observations and chemistry, *Chemical Society  
Reviews*, 41, 6405-6447, 2012.
- Brown, S. S., Dibb, J. E., Stark, H., Aldener, M., Vozella, M., Whitlow, S., Williams, E. J.,  
Lerner, B. M., Jakoubek, R., Middlebrook, A. M., DeGouw, J. A., Warneke, C., Goldan, P.  
D., Kuster, W. C., Angevine, W. M., Sueper, D. T., Quinn, P. K., Bates, T. S., Meagher, J. F.,  
Fehsenfeld, F. C., and Ravishankara, A. R.: Nighttime removal of  $\text{NO}_x$  in the summer marine  
boundary layer, *Geophysical Research Letters*, 31, L07108-L07113, 2004.

31 Brown, S. S., Osthoff, H. D., Stark, H., Dubé, W. P., Ryerson, T. B., Warneke, C., de Gouw,  
 32 J. A., Wollny, A. G., Parrish, D. D., Fehsenfeld, F. C., Ravishankara, A. R.: Aircraft  
 33 observations of daytime NO<sub>3</sub> and N<sub>2</sub>O<sub>5</sub> and their implications for tropospheric chemistry,  
 34 Journal of Photochemistry and Photobiology A: Chemistry, 176, 270-278, 2005.

35 Brown, S. S., Ryerson, T. B., Wollny, A. G., Brock, C. A., Peltier, R., Sullivan, A. P., Weber,  
 36 R. J., Dubé, W. P., Trainer, M., Meagher, J. F., Fehsenfeld, F. C., and Ravishankara, A. R.:  
 37 Variability in Nocturnal Nitrogen Oxide Processing and Its Role in Regional Air Quality,  
 38 Science, 311, 67-70, 2006.

39 Brown, S. S., Dubé, W. P., Peischl, J., Ryerson, T., Atlas, E., Warneke, C., de Gouw, J. A., te  
 40 Lintel Hekkert, S., Brock, C. A., Flocke, F., Trainer, M., Parrish, D. D., Feshenfeld, F. C., and  
 41 Ravishankara, A.: Budgets for nocturnal VOC oxidation by nitrate radicals aloft during the  
 42 2006 Texas Air Quality Study, Journal of Geophysical Research: Atmospheres, 116, D24305-  
 43 D24320, 2011.

44 Cantrell, C. A., Zimmer, A., and Tyndall, G. S.: Absorption cross sections for water vapor  
 45 from 183 to 193 nm, Geophysical Research Letters, 24, 2195-2198, 1997.

46 Carter, W. P. L., and Atkinson, R.: Alkyl Nitrate Formation from the Atmospheric  
 47 Photooxidation of Alkanes; a Revised Estimation Method, Journal of Atmospheric Chemistry,  
 48 8, 165-173, 1989.

49 Commane, R.: Understanding Radical Chemistry Throughout the Troposphere using Laser-  
 50 Induced Fluorescence Spectroscopy, PhD, Chemistry, University of Leeds, Leeds, 2009.

51 Commane, R., Floquet, C. F. A., Ingham, T., Stone, D., Evans, M. J., and Heard, D. E.:  
 52 Observations of OH and HO<sub>2</sub> radicals over West Africa, Atmospheric Chemistry and Physics,  
 53 10, 8783-8801, 2010.

54 Creasey, D. J., Halford-Maw, P. A., Heard, D. E., Pilling, M. J., and Whitaker, B. J.:  
 55 Implementation and initial deployment of a field instrument for measurement of OH and HO<sub>2</sub>  
 56 in the troposphere by laser-induced fluorescence, J. Chem. Soc.-Faraday Trans., 93, 2907-  
 57 2913, 1997.

58 Creasey, D. J., Heard, D. E., and Lee, J. D.: Eastern Atlantic Spring Experiment 1997  
 59 (EASE97) 1. Measurements of OH and HO<sub>2</sub> concentrations at Mace Head, Ireland, Journal of  
 60 Geophysical Research: Atmospheres, 107, 4091-4106, 2002.

61 Dari-Salisburgo, C., Di Carlo, P., Giammaria, F., Kajii, Y., and D'Altorio, A.: Laser induced  
62 fluorescence instrument for NO<sub>2</sub> measurements: Observations at a central Italy background  
63 site, *Atmospheric Environment*, 43, 970-977, 2009.

64 Di Carlo, P., Aruffo, E., Busilacchio, M., Giammaria, F., Dari-Salisburgo, C., Biancofiore, F.,  
65 Visconti, G., Lee, J., Moller, S., Reeves, C. E., Baugitte, S., Forster, G., Jones, R. L., and  
66 Ouyang, B.: Aircraft based four-channel thermal dissociation laser induced fluorescence  
67 instrument for simultaneous measurements of NO<sub>2</sub>, total peroxy nitrate, total alkyl nitrate, and  
68 HNO<sub>3</sub>, *Atmospheric Measurement Techniques*, 6, 971-980, 2013.

69 Donahue, N. M., Kroll, J. H., Anderson, J. G., and Demerjian, K. L.: Direct observation of  
70 OH production from the ozonolysis of olefins, *Geophysical Research Letters*, 25, 59-62, 1998.

71 Donahue, N. M., Drozd, G. T., Epstein, S. A., Presto, A. A., and Kroll, J. H.: Adventures in  
72 ozoneland: down the rabbit-hole, *Physical Chemistry Chemical Physics*, 13, 10848-10857,  
73 2011.

74 Drozd, G. T., and Donahue, N. M.: Pressure Dependence of Stabilized Criegee Intermediate  
75 Formation from a Sequence of Alkenes, *Journal of Physical Chemistry A*, 115, 4381-4387,  
76 2011.

77 Dusanter, S., Vimal, D., Stevens, P. S., Volkamer, R., and Molina, L. T.: Measurements of  
78 OH and HO<sub>2</sub> concentrations during the MCMA-2006 field campaign - Part 1: Deployment of  
79 the Indiana University laser-induced fluorescence instrument, *Atmospheric Chemistry and*  
80 *Physics*, 9, 1665-1685, 2009.

81 Edwards, G. D., Cantrell, C., Stephens, S., Hill, B., Goyea, O., Shetter, R., Mauldin, R. L.,  
82 Kosciuch, E., Tanner, D., and Eisele, F.: Chemical Ionization Mass Spectrometer Instrument  
83 for the Measurement of Tropospheric HO<sub>2</sub> and RO<sub>2</sub>, *Analytical Chemistry*, 75, 5317-5327,  
84 2003.

85 Emmerson, K. M., and Carslaw, N.: Night-time radical chemistry during the TORCH  
86 campaign, *Atmospheric Environment*, 43, 3220-3226, 2009.

87 Emmerson, K. M., and Evans, M. J.: Comparison of tropospheric gas-phase chemistry  
88 schemes for use within global models, *Atmospheric Chemistry and Physics*, 9, 1831-1845,  
89 2009.

90 Emmerson, K. M., Carslaw, N., and Pilling, M. J.: Urban Atmospheric Chemistry During the  
 91 PUMA Campaign 2: Radical Budgets for OH, HO<sub>2</sub> and RO<sub>2</sub>, Journal of Atmospheric  
 92 Chemistry, 52, 165-183, 2005.

93 Emmerson, K. M., Carslaw, N., Carslaw, D. C., Lee, J. D., McFiggans, G., Bloss, W. J.,  
 94 Gravestock, T., Heard, D. E., Hopkins, J., Ingham, T., Pilling, M. J., Smith, S. C., Jacob, M.,  
 95 and Monks, P. S.: Free radical modelling studies during the UK TORCH Campaign in  
 96 Summer 2003, Atmospheric Chemistry and Physics, 7, 167-181, 2007.

97 Faloon, I. C., Tan, D., Leshner, R. L., Hazen, N. L., Frame, C. L., Simpas, J. B., Harder, H.,  
 98 Martinez, M., di Carlo, P., Ren, X., and Brune, W. H.: A Laser-Induced Fluorescence  
 99 Instrument for Detecting Tropospheric OH and HO<sub>2</sub>: Characteristics and Calibration, Journal  
 100 of Atmospheric Chemistry, 47, 139-167, 2004.

101 Fleming, Z. L., Monks, P. S., Rickard, A. R., Heard, D. E., Bloss, W. J., Seakins, P. W., Still,  
 102 T. J., Sommariva, R., Pilling, M. J., Morgan, R., Green, T. J., Brough, N., Mills, G. P.,  
 103 Penkett, S. A., Lewis, A. C., Lee, J. D., Saiz-Lopez, A., and Plane, J. M. C.: Peroxy radical  
 104 chemistry and the control of ozone photochemistry at Mace Head, Ireland during the summer  
 105 of 2002, Atmospheric Chemistry and Physics, 6, 2193-2214, 2006.

106 Floquet, C. F. A.: Airborne Measurements of Hydroxyl Radicals by Fluorescence Assay by  
 107 Gas Expansion, PhD, School of Chemistry, University of Leeds, Leeds, 155 pp., 2006.

108 Fuchs, H., Bohn, B., Hofzumahaus, A., Holland, F., Lu, K. D., Nehr, S., Rohrer, F., and  
 109 Wahner, A.: Detection of HO<sub>2</sub> by laser-induced fluorescence: Calibration and interferences  
 110 from RO<sub>2</sub> radicals, Atmospheric Measurement Techniques, 4, 1255-1302, 2011.

111 Gerbig, C., Schmitgen, S., Kley, D., and Volz-Thomas, A.: An improved fast-response  
 112 vacuum-UV resonance fluorescence CO instrument, Journal of Geophysical Research:  
 113 Atmospheres, 104, 1699-1704, 1999.

114 German, K. R.: Direct measurement of the radiative lifetimes of the A<sup>2</sup>Σ<sup>+</sup> (V'=0), Journal of  
 115 Chemical Physics, 62, 2584-2587, 1975.

116 Geyer, A., and Stutz, J.: The vertical structure of OH-HO<sub>2</sub>-RO<sub>2</sub> chemistry in the nocturnal  
 117 boundary layer: A one-dimensional model study, Journal of Geophysical Research:  
 118 Atmospheres, 109, D16301-D16316, 2004a.

119 Geyer, A., and Stutz, J.: Vertical profiles of  $\text{NO}_3$ ,  $\text{N}_2\text{O}_5$ ,  $\text{O}_3$ , and  $\text{NO}_x$  in the nocturnal  
 120 boundary layer: 2. Model studies on the altitude dependence of composition and chemistry,  
 121 Journal of Geophysical Research: Atmospheres, 109, D12307, doi:10.1029/2003JD004211,  
 122 2004b.

123 Geyer, A., Bächmann, K., Hofzumahaus, A., Holland, F., Konrad, S., Klüpfel, T., Pätz, H.-  
 124 W., Perner, D., Mihelcic, D., Schäfer, H.-J., Volz-Thomas, A., and Platt, U.: Nighttime  
 125 formation of peroxy and hydroxyl radicals during the BERLIOZ campaign: Observations and  
 126 modeling studies, Journal of Geophysical Research: Atmospheres, 108, 8249-8263, 2003.

127 Harrison, R. M., Yin, J., Tilling, R. M., Cai, X., Seakins, P. W., Hopkins, J. R., Lansley, D.  
 128 L., Lewis, A. C., Hunter, M. C., Heard, D. E., Carpenter, L. J., Creasey, D. J., Lee, J. D.,  
 129 Pilling, M. J., Carslaw, N., Emmerson, K. M., Redington, A., Derwent, R. G., Ryall, D.,  
 130 Mills, G., and Penkett, S. A.: Measurement and modelling of air pollution and atmospheric  
 131 chemistry in the U.K. West Midlands conurbation: Overview of the PUMA Consortium  
 132 project, Science of the Total Environment, 360, 5-25, 2006.

133 Heard, D. E.: Atmospheric field measurements of the hydroxyl radical using laser-induced  
 134 fluorescence spectroscopy, Annual Review of Physical Chemistry, 57, 191–216, 2006.

135 Heard, D. E., Carpenter, L. J., Creasey, D. J., Hopkins, J. R., Lee, J. D., Lewis, A. C., Pilling,  
 136 M. J., Seakins, P. W., Carslaw, N., and Emmerson, K. M.: High levels of the hydroxyl radical  
 137 in the winter urban troposphere, Geophysical Research Letters, 31, L18112-L18117,  
 138 10.1029/2004gl020544, 2004.

139 Hewitt, C. N., Lee, J. D., MacKenzie, A. R., Barkley, M. P., Carslaw, N., Carver, G. D.,  
 140 Chappell, N. A., Coe, H., Collier, C., Commane, R., Davies, F., Davison, B., Di Carlo, P., Di  
 141 Marco, C. F., Dorsey, J. R., Edwards, P. M., Evans, M. J., Fowler, D., Furneaux, K. L.,  
 142 Gallagher, M., Guenther, A., Heard, D. E., Helfter, C., Hopkins, J., Ingham, T., Irwin, M.,  
 143 Jones, C., Karunaharan, A., Langford, B., Lewis, A. C., Lim, S. F., MacDonald, S. M.,  
 144 Mahajan, A. S., Malpass, S., McFiggans, G., Mills, G., Misztal, P., Moller, S., Monks, P. S.,  
 145 Nemitz, E., Nicolas-Perea, V., Oetjen, H., Oram, D. E., Palmer, P. I., Phillips, G. J., Pike, R.,  
 146 Plane, J. M. C., Pugh, T., Pyle, J. A., Reeves, C. E., Robinson, N. H., Stewart, D., Stone, D.,  
 147 Whalley, L. K., and Yin, X.: Overview: oxidant and particle photochemical processes above a  
 148 south-east Asian tropical rainforest (the OP3 project): introduction, rationale, location  
 149 characteristics and tools, Atmospheric Chemistry and Physics, 10, 169-199, 2010.

150 Holland, F., Hofzumahaus, A., Schäfer, J., Kraus, A., and Pätz, H.-W.: Measurements of OH  
 151 and HO<sub>2</sub> radical concentrations and photolysis frequencies during BERLIOZ, Journal of  
 152 Geophysical Research: Atmospheres, 108, 8246-8261, 2003.

153 Hopkins, J. R., Lewis, A. C., and Read, K. A.: A two-column method for long-term  
 154 monitoring of non-methane hydrocarbons (NMHCs) and oxygenated volatile organic  
 155 compounds (*o*-VOCs), Journal of Environmental Monitoring, 5, 8-13, 2003.

156 Jenkin, M. E., Saunders, S. M., and Pilling, M. J.: The tropospheric degradation of volatile  
 157 organic compounds: A protocol for mechanism development, Atmospheric Environment, 31,  
 158 81-104, 1997.

159 Jenkin, M. E., Saunders, S. M., Wagner, V., and Pilling, M. J.: Protocol for the development  
 160 of the Master Chemical Mechanism, MCM v3 (Part B): tropospheric degradation of aromatic  
 161 volatile organic compounds, Atmospheric Chemistry and Physics, 3, 181-193, 2003.

162 Johnson, D., and Marston, G.: The gas-phase ozonolysis of unsaturated volatile organic  
 163 compounds in the troposphere, Chemical Society Reviews, 37, 699–716, 2008.

164 Jones, A. R., Thomson, D. J., Hort, M., and Devenish, B.: The U.K. Met Office's next-  
 165 generation atmospheric dispersion model, NAME III, in: Air Pollution Modeling and its  
 166 Application XVII (Proceedings of the 27th NATO/CCMS International Technical Meeting on  
 167 Air Pollution Modelling and its Application), edited by: Borrego, C., and Norman, A.-L.,  
 168 Springer, Dordrecht, Netherlands, 580-589, 2007.

169 Kanaya, Y., Sadanaga, Y., Matsumoto, J., Sharma, U. K., Hirokawa, J., Kajii, Y., and  
 170 Akimoto, H.: Nighttime observation of the HO<sub>2</sub> radical by an LIF instrument at Oki Island,  
 171 Japan, and its possible origins, Geophysical Research Letters, 26, 2179-2182, 1999.

172 Kennedy, O. J., Ouyang, B., Langridge, J. M., Daniels, M. J. S., Baugitte, S., Freshwater, R.,  
 173 McLeod, M. W., Ironmonger, C., Sendall, J., Norris, O., Nightingale, R., Ball, S. M., and  
 174 Jones, R. L.: An aircraft based three channel broadband cavity enhanced absorption  
 175 spectrometer for simultaneous measurements of NO<sub>3</sub>, N<sub>2</sub>O<sub>5</sub> and NO<sub>2</sub>, Atmospheric  
 176 Measurement Techniques, 4, 1759-1776, 2011.

177 Kroll, J. H., Clarke, J. S., Donahue, N. M., Anderson, J. G., and Demerjian, K. L.: Mechanism  
 178 of HO<sub>x</sub> Formation in the Gas-Phase Ozone-Alkene reaction. 1. Direct, Pressure-Dependent  
 179 Measurements of Prompt OH Yields, J. Phys. Chem. A, 105, 1554-1560, 2001a.

180 Kroll, J. H., Sahay, S. R., Anderson, J. G., Demerjian, K. L., and Donahue, N. M.:  
 181 Mechanism of HO<sub>x</sub> Formation in the Gas-Phase Ozone-Alkene Reaction. 2. Prompt versus  
 182 Thermal Dissociation of Carbonyl Oxides to Form OH, *Journal of Physical Chemistry A*,  
 183 105, 4446-4457 2001b.

184 Kroll, J. H., Donahue, N. M., Cee, V. J., Demerjian, K. L., and Anderson, J. G.: Gas-Phase  
 185 Ozonolysis of Alkenes: Formation of OH from Anti Carbonyl Oxides, *Journal of the*  
 186 *American Chemical Society*, 124, 8518-8519, 2002.

187 Lee, J. D., Lewis, A. C., Monks, P. S., Jacob, M., Hamilton, J. F., Hopkins, J. R., Watson, N.  
 188 M., Saxton, J. E., Ennis, C., Carpenter, L. J., Carslaw, N., Fleming, Z. L., Bandy, A., Oram,  
 189 D. E., Penkett, S. A., Slemr, J., Norton, E. G., Rickard, A. R., Whalley, L. K., Heard, D. E.,  
 190 Bloss, W. J., Gravestock, T., Smith, S. C., Stanton, J., Pilling, M. J., and Jenkin, M. E.: Ozone  
 191 photochemistry and elevated isoprene during the UK heatwave of August 2003, *Atmospheric*  
 192 *Environment*, 40, 7598– 7613, 2006.

193 Lidster, R. T., Hamilton, J. F., Lee, J. D., Lewis, A. C., Hopkins, J. R., Punjabi, S., Rickard,  
 194 A. R., and Young, J. C.: The impact of monoaromatic hydrocarbons on OH reactivity in the  
 195 coastal UK boundary layer and free troposphere, *Atmospheric Chemistry and Physics*, 14,  
 196 6677-6693, 2014.

197 Lightfoot, P. D., Cox, R. A., Crowley, J. N., Destriau, M., Hayman, G. D., Jenkin, M. E.,  
 198 Moortgat, G. K., and Zabel, F.: Organic Peroxy Radicals: Kinetics, Spectroscopy and  
 199 Tropospheric Chemistry, *Atmospheric Environment*, 26A, 1805-1961, 1992.

200 Lou, S., Holland, F., Rohrer, F., Lu, K., Bohn, B., Brauers, T., Chang, C. C., Fuchs, H.,  
 201 Häsel, R., Kita, K., Kondo, Y., Li, X., Shao, M., Zeng, L., Wahner, A., Zhang, Y., Wang,  
 202 W., and Hofzumahaus, A.: Atmospheric OH reactivities in the Pearl River Delta - China in  
 203 summer 2006: measurement and model results, *Atmospheric Chemistry and Physics*, 10,  
 204 11243-11260, 10.5194/acp-10-11243, 2010.

205 Lu, K. D., Rohrer, F., Holland, F., Fuchs, H., Bohn, B., Brauers, T., Chang, C. C., Häsel, R.,  
 206 Hu, M., Kita, K., Kondo, Y., Li, X., Lou, S. R., Nehr, S., Shao, M., Zeng, L. M., Wahner, A.,  
 207 Zhang, Y. H., and Hofzumahaus, A.: Observation and modelling of OH and HO<sub>2</sub>  
 208 concentrations in the Pearl River Delta 2006: a missing OH source in a VOC rich atmosphere,  
 209 *Atmospheric Chemistry and Physics*, 12, 1541-1569, 2012.



210 Lu, K. D., Hofzumahaus, A., Holland, F., Bohn, B., Brauers, T., Fuchs, H., Hu, M., Häseler,  
 211 R., Kita, K., Kondo, Y., Li, X., Lou, S. R., Oebel, A., Shao, M., Zeng, L. M., Wahner, A.,  
 212 Zhu, T., Zhang, Y. H., and Rohrer, F.: Missing OH source in a suburban environment near  
 213 Beijing: observed and modelled OH and HO<sub>2</sub> concentrations in summer 2006, *Atmospheric*  
 214 *Chemistry and Physics*, 13, 1057-1080, 2013.

215 Lu, K., Rohrer, F., Holland, F., Fuchs, H., Brauers, T., Oebel, A., Dlugi, R., Hu, M., Li, X.,  
 216 Lou, S., Shao, M., Zhu, T., Wahner, A., Zhang, Y., and Hofzumahaus, A.: Nighttime  
 217 observation and chemistry of HO<sub>x</sub> in the Pearl River Delta and Beijing in summer 2006,  
 218 *Atmospheric Chemistry and Physics*, 14, 4979-4999, doi:10.5194/acp-14-4979-2014, 2014.

219 Martinez, M., Harder, H., Kubistin, D., Rudolf, M., Bozem, H., Eerdeken, G., Fischer, H.,  
 220 Klüpfel, T., Gurk, C., Königstedt, R., Parchatka, U., Schiller, C. L., Stickler, A., Williams, J.,  
 221 and Lelieveld, J.: Hydroxyl radicals in the tropical troposphere over the Suriname rainforest:  
 222 airborne measurements, *Atmospheric Chemistry and Physics*, 10, 3759-3773, 10.5194/acp-10-  
 223 3759, 2010.

224 Mauldin III, R. L., Berndt, T., Sipilä, M., Paasonen, P., Petäjä, T., Kim, S., Kurtén, A.,  
 225 Stratmann, F., Kerminen, V.-M., and Kulmala, M.: A new atmospherically relevant oxidant of  
 226 sulphur dioxide, *Nature*, 488, 193-196, 2012.

227 Morgan, W. T., Ouyang, B., Allan, B. J., Aruffo, E., Di Carlo, P., Kennedy, O. J., Lowe, D.,  
 228 Flynn, M. J., Rosenberg, P. D., Williams, P. I., Jones, R., McFiggans, G. B., and Coe, H.:  
 229 Influence of aerosol chemical composition on N<sub>2</sub>O<sub>5</sub> uptake: airborne regional measurements  
 230 in North-Western Europe, *Atmospheric Chemistry and Physics Discussions*, 14, 19673-  
 231 19718, 2014.

232 Nakajima, M., and Endo, Y.: Determination of the molecular structure of the simplest Criegee  
 233 intermediate CH<sub>2</sub>OO, *Journal of Chemical Physics*, 139, 101103, doi:10.1063/1.4821165,  
 234 2013.

235 Nakajima, M., and Endo, Y.: Spectroscopic characterization of an alkyl substituted Criegee  
 236 intermediate *syn*-CH<sub>3</sub>CHOO through pure rotational transitions, *Journal of Chemical Physics*,  
 237 140, 011101, doi:10.1063/1.4861494, 2014.

238 Ouyang, B., McLeod, M. W., Jones, R. L., and Bloss, W. J.: NO<sub>3</sub> radical production from the  
 239 reaction between the Criegee intermediate CH<sub>2</sub>OO and NO<sub>2</sub>, *Physical Chemistry Chemical*  
 240 *Physics*, 15, 17070-17075, 2013.

241 Paulson, S. E., and Orlando, J. J.: The reactions of ozone with alkenes: An important source  
 242 of HO<sub>x</sub> in the boundary layer, *Geophysical Research Letters*, 23, 3727-3730, 1996.

243 Ren, X., Harder, H., Martinez, M., Leshner, R., Oliger, A., Simpasa, J. B., Brune, W. H.,  
 244 Schwab, J. J., Demerjian, K. L., He, Y., Zhou, X., and Gao, H.: OH and HO<sub>2</sub> chemistry in the  
 245 urban atmosphere of New York City, *Atmospheric Environment*, 37, 3639-3651, 2003a.

246 Ren, X., Harder, H., Martinez, M., Leshner, R. L., Oliger, A., Shirley, T., Adams, J., Simpasa, J.  
 247 B., and Brune, W. H.: HO<sub>x</sub> concentrations and OH reactivity observations in New York City  
 248 during PMTACS-NY2001, *Atmospheric Environment*, 37, 3627-3637, 2003b.

249 Ren, X., Brune, W. H., Mao, J., Mitchell, M. J., Leshner, R., Simpasa, J. B., Metcalf, A. R.,  
 250 Schwab, J. J., Cai, C., Li, Y., Demerjian, K. L., Felton, H. D., Boynton, G., Adams, A., Perry,  
 251 J., He, Y., Zhou, X., and Hou, J.: Behavior of OH and HO<sub>2</sub> in the winter atmosphere in New  
 252 York City, *Atmospheric Environment*, 40, 252-263, 2006.

253 Salisbury, G., Rickard, A. R., Monks, P. S., Allan, B. J., Bauguutte, S. J. B., Penkett, S. A.,  
 254 Carslaw, N., Lewis, A. C., Creasey, D. J., Heard, D. E., Jacobs, P. J., and Lee, J. D.:  
 255 Production of peroxy radicals at night via reactions of ozone and the nitrate radical in the  
 256 marine boundary layer, *Journal of Geophysical Research: Atmospheres*, 106, 12669-12687,  
 257 2001.

258 Saunders, S. M., Jenkin, M. E., Derwent, R. G., and Pilling, M. J.: Protocol for the  
 259 development of the Master Chemical Mechanism, MCM v3 (Part A): tropospheric  
 260 degradation of non-aromatic volatile organic compounds, *Atmospheric Chemistry and*  
 261 *Physics*, 3, 161-180, 2003.

262 Sheehy, P. M., Volkamer, R., Molina, L. T., and Molina, M. J.: Oxidative capacity of the  
 263 Mexico City atmosphere - Part 2: A RO<sub>x</sub> radical cycling perspective, *Atmospheric Chemistry*  
 264 *and Physics*, 10, 6993-7008, 2010.

265 Shirley, T. R., Brune, W. H., Ren, X., Mao, J., Leshner, R., Cardenas, B., Volkamer, R.,  
 266 Molina, L. T., Molina, M. J., Lamb, B., Velasco, E., Jobson, T., and Alexander, M.:  
 267 Atmospheric oxidation in the Mexico City Metropolitan Area (MCMA) during April 2003,  
 268 *Atmospheric Chemistry and Physics*, 6, 2753-2765, 2006.

269 Smith, S. C., Lee, J. D., Bloss, W. J., Johnson, G. P., Ingham, T., and Heard, D. E.:  
 270 Concentrations of OH and HO<sub>2</sub> radicals during NAMBLEX: measurements and steady state  
 271 analysis, *Atmospheric Chemistry and Physics*, 6, 1435-1453, 2006.

272 Sommariva, R., Pilling, M. J., Bloss, W. J., Heard, D. E., Lee, J. D., Fleming, Z. L., Monks,  
 273 P. S., Plane, J. M. C., Saiz-Lopez, A., Ball, S. M., Bitter, M., Jones, R. L., Brough, N.,  
 274 Penkett, S. A., Hopkins, J. R., Lewis, A. C., and Read, K. A.: Night-time radical chemistry  
 275 during the NAMBLEX campaign, *Atmospheric Chemistry and Physics*, 7, 587-598, 2007.

276 Sommariva, R., Osthoff, H. D., Brown, S. S., Bates, T. S., Baynard, T., Coffman, D., de  
 277 Gouw, J. A., Goldan, P. D., Kuster, W. C., Lerner, B. M., Stark, H., Warneke, C., Williams,  
 278 E. J., Fehsenfeld, F. C., Ravishankara, A. R., and Trainer, M.: Radicals in the marine  
 279 boundary layer during NEAQS 2004: a model study of day-time and night-time sources and  
 280 sinks, *Atmospheric Chemistry and Physics*, 9, 3075-3093, 2009.

281 Stewart, D. J., Taylor, C. M., Reeves, C. E., and McQuaid, J.: Biogenic nitrogen oxide  
 282 emissions from soils: impact on NO<sub>x</sub> and ozone over west Afric during AMMA (African  
 283 Monsoon Multidisciplinary Analysis): observational study, *Atmospheric Chemistry and*  
 284 *Physics*, 8, 2285-2297, 2008.

285 Still, T. J., Al-Haider, S., Seakins, P. W., Sommariva, R., Stanton, J. C., Mills, G., and  
 286 Penkett, S. A.: Ambient formaldehyde measurements made at a remote marine boundary layer  
 287 site during the NAMBLEX campaign - a comparison of data from chromatographic and  
 288 modified Hantzsch techniques., *Atmospheric Chemistry and Physics*, 6, 2711-2726, 2006.

289 Stone, D., Evans, M. J., Commane, R., Ingham, T., Floquet, C. F. A., McQuaid, J. B.,  
 290 Brookes, D. M., Monks, P. S., Purvis, R., Hamilton, J. F., Hopkins, J., Lee, J., Lewis, A. C.,  
 291 Stewart, D., Murphy, J. G., Mills, G., Oram, D., Reeves, C. E., and Heard, D. E.: HO<sub>x</sub>  
 292 observations over West Africa during AMMA: impact of isoprene and NO<sub>x</sub>, *Atmospheric*  
 293 *Chemistry and Physics*, 10, 9415-9429, 2010.

294 Stone, D., Whalley, L. K., and Heard, D. E.: Tropospheric OH and HO<sub>2</sub> radicals: field  
 295 measurements and model comparisons, *Chemical Society Reviews*, 41, 6348-6404, 2012.

296 Stone, D., Blitz, M., Daubney, L., Howes, N. U. M., and Seakins, P.: Kinetics of CH<sub>2</sub>OO  
 297 reactions with SO<sub>2</sub>, NO<sub>2</sub>, NO, H<sub>2</sub>O and CH<sub>3</sub>CHO as a function of pressure, *Physical*  
 298 *Chemistry Chemical Physics*, 16, 1139-1149, 2014a.

299 Stone, D., Evans, M. J., Walker, H. M., Ingham, T., Vaughan, S., Ouyang, B., Kennedy, O. J.,  
 300 McLeod, M. W., Jones, R. L., Hopkins, J., Punjabi, S., Lidster, R., Hamilton, J. F., Lee, J. D.,  
 301 Lewis, A. C., Carpenter, L. J., Forster, G., Oram, D., Reeves, C. E., Baugitte, S., Morgan, W.,  
 302 Coe, H., Aruffo, E., Dari-Salisburgo, C., Giammaria, F., Di Carlo, P., and Heard, D. E.:  
 303 Radical chemistry at night: comparisons between observed and modelled HO<sub>x</sub>, NO<sub>3</sub> and N<sub>2</sub>O<sub>5</sub>  
 304 during the RONOCO project, *Atmospheric Chemistry and Physics*, 14, 1299-1321, 2014b.

305 Stutz, J., Alicke, B., Ackermann, R., Geyer, A., White, A., and Williams, E.: Vertical profiles  
 306 of NO<sub>3</sub>, N<sub>2</sub>O<sub>5</sub>, O<sub>3</sub>, and NO<sub>x</sub> in the nocturnal boundary layer: 1. Observations during the Texas  
 307 Air Quality Study 2000, *Journal of Geophysical Research: Atmospheres*, 109, D12306-  
 308 D12320, 2004.

309 Su, Y.-T., Huang, Y.-H., Witek, H. A., and Lee, Y.-P.: Infrared Absorption Spectrum of the  
 310 Simplest Criegee Intermediate CH<sub>2</sub>OO, *Science*, 340, 174-176, 2013.

311 Taatjes, C. A., Meloni, G., Selby, T. M., Trevitt, A. J., Osborn, D. L., Percival, C. J., and  
 312 Shallcross, D. E.: Direct Observation of the Gas-Phase Criegee Intermediate (CH<sub>2</sub>OO),  
 313 *Journal of the American Chemical Society*, 130, 11883-11885, 2008.

314 Taatjes, C. A., Welz, O., Eskola, A. J., Savee, J. D., Osborn, D. L., Lee, E. P. F., Dyke, J. M.,  
 315 Mok, D. W. K., Shallcross, D. E., and Percival, C. J.: Direct measurement of Criegee  
 316 intermediate (CH<sub>2</sub>OO) reactions with acetone, acetaldehyde, and hexafluoroacetone, *Physical  
 317 Chemistry Chemical Physics*, 14, 10391-10400, 2012.

318 Taatjes, C. A., Welz, O., Eskola, A. J., Savee, J. D., Scheer, A. M., Shallcross, D. E.,  
 319 Rotavera, B., Lee, E. P. F., Dyke, J. M., Mok, D. W. K., Osborn, D. L., and Percival, C. J.:  
 320 Direct Measurements of Conformer-Dependent Reactivity of the Criegee Intermediate  
 321 CH<sub>3</sub>CHOO, *Science*, 340, 177-180, 2013.

322 Taatjes, C. A., Shallcross, D. E., and Percival, C. J.: Research frontiers in the chemistry of  
 323 Criegee intermediates and tropospheric ozonolysis, *Physical Chemistry Chemical Physics*, 16,  
 324 1689-2180, 2014.

325 Vereecken, L., and Francisco, J. S.: Theoretical studies of atmospheric reaction mechanisms  
 326 in the troposphere, *Chemical Society Reviews*, 41, 6217-6708, 2012.

327 Volkamer, R., Sheehy, P., Molina, L. T., and Molina, M. J.: Oxidative capacity of the Mexico  
 328 City atmosphere - Part 1: A radical source perspective, *Atmospheric Chemistry and Physics*,  
 329 10, 6969-6991, 2010.

330 Welz, O., Savee, J. D., Osborn, D. L., Vasu, S. S., Percival, C. J., Shallcross, D. E., and  
 331 Taatjes, C. A.: Direct Kinetic Measurements of Criegee Intermediate ( $\text{CH}_2\text{OO}$ ) Formed by  
 332 Reaction of  $\text{CH}_2\text{I}$  with  $\text{O}_2$ , *Science*, 335, 204-207, 2012.

333 Whalley, L. K., Furneaux, K. L., Goddard, A., Lee, J. D., Mahajan, A., Oetjen, H., Read, K.  
 334 A., Kaaden, N., Carpenter, L. J., Lewis, A. C., Plane, J. M. C., Saltzman, E. S., Wiedensohler,  
 335 A., and Heard, D. E.: The chemistry of OH and  $\text{HO}_2$  radicals in the boundary layer over the  
 336 tropical Atlantic Ocean, *Atmospheric Chemistry and Physics*, 10, 1555-1576, 2010.

337 Whalley, L. K., Blitz, M. A., Desservettaz, M., Seakins, P. W., and Heard, D. E.: Reporting  
 338 the sensitivity of Laser Induced Fluorescence instruments used for  $\text{HO}_2$  detection to an  
 339 interference from  $\text{RO}_2$  radicals and introducing a novel approach that enables  $\text{HO}_2$  and certain  
 340  $\text{RO}_2$  types to be selectively measured, *Atmospheric Measurement Techniques*, 6, 3425-3440,  
 341 2013.

342 Winiberg, F. A. F., Smith, S. C., Bejan, I., Brumby, C. A., Ingham, T., Malkin, T. L., Orr, S.  
 343 C., Heard, D. E., and Seakins, P. W.: Pressure dependent calibration of the OH and  $\text{HO}_x$   
 344 channels of a FAGE  $\text{HO}_x$  instrument using the Highly Instrumented Reactor for Atmospheric  
 345 Chemistry (HIRAC), *Atmospheric Measurement Techniques Discussions*, 7, 7963-8011,  
 346 2014.

347 Wong, K. W., and Stutz, J.: Influence of nocturnal vertical stability on daytime chemistry: A  
 348 one-dimensional model study, *Atmospheric Environment*, 44, 3753-3760, 2010.

1 Table 1. Examples of modelling studies and observations of HO<sub>x</sub> radicals and VOC oxidation at night. PERCA = Peroxy Radical Chemical  
2 Amplification; LIF = Laser Induced Fluorescence; DOAS = Differential Optical Absorption Spectroscopy; MCM = Master Chemical Mechanism;  
3 MIESR = Matrix Isolation Electron Spin Resonance; RACM = Regional Atmospheric Chemistry Mechanism; CRDS = Cavity Ring Down  
4 Spectroscopy; CIMS = Chemical Ionisation Mass Spectrometry; GC = Gas Chromatography; PTRMS = Proton Transfer Reaction Mass Spectrometry;  
5 FTIR = Fourier Transform Infrared Spectroscopy; DUALER (DUAL channel peroxy radical chemical amplifier); OA-CRD = Off Axis Cavity Ring  
6 Down Spectroscopy; CRM-PTR-MS = Comparative Reactivity Method Proton Transfer Mass Spectrometry.

| Location,<br>Campaign,<br>Date             | Methods   | Results   | Reference  |
|--|---|---|--|
| Mace Head,<br>Ireland,<br>EASE97,<br>1997  | Measurements: [HO <sub>2</sub> +RO <sub>2</sub> ] measured by PERCA;<br>HO <sub>x</sub> measured by LIF; NO <sub>3</sub> measured by DOAS).<br>Modelling: Campaign-tailored box model<br>constrained to measurements, based on MCM. | 2 nights of HO <sub>x</sub> measurements: HO <sub>2</sub> = 1–2 and 0.5–0.7 pptv; OH<br>not detected above limit of detection ( $\sim 2.5 \times 10^5 \text{ cm}^{-3}$ ). NO <sub>3</sub><br>dominated radical production in westerly (clean) air masses; O <sub>3</sub><br>dominated in NE, SE, and SW air masses and dominated radical<br>production overall during the campaign.   | Salisbury et al.<br>(2001); Creasey et<br>al. (2002) |
| Pabstthum,<br>Germany,<br>BERLIOZ<br>1998, | Measurements: HO <sub>x</sub> measured by LIF; NO <sub>3</sub><br>measured by DOAS and MIESR. Modelling:<br>Zero-dimensional model using lumped VOC<br>reactivity, constrained to measured species.                                 | Nighttime OH = $1.85 \times 10^5 \text{ cm}^{-3}$ , compared to modelled value<br>of $4.1 \times 10^5 \text{ cm}^{-3}$ . Nighttime HO <sub>2</sub> = $3 \times 10^7 \text{ cm}^{-3}$ , model results in<br>agreement. NO <sub>3</sub> chemistry responsible for 53 % of HO <sub>2</sub> and 36 % of<br>OH during the night. O <sub>3</sub> + alkene responsible for 47 % of HO <sub>2</sub> and<br>64 % of OH during the night. | Geyer et al.<br>(2003); Holland et<br>al. (2003)     |
| Birmingham,<br>PUMA, 1999<br>and 2000      | Measurements: HO <sub>x</sub> measured by LIF. Modelling:<br>Photochemical box model constrained to<br>measurements, based on MCM.  | Daytime OH initiation dominated by O <sub>3</sub> + alkenes, HONO<br>photolysis, and O( <sup>1</sup> D) + H <sub>2</sub> O during summer. O <sub>3</sub> + alkenes<br>dominated in winter. O <sub>3</sub> + alkenes main radical source at night.   | Emmerson et al.<br>(2005); Harrison et<br>al. (2006) |
| New York,<br>PMTACS-<br>NY, 2001           | Measurements: HO <sub>x</sub> measured by LIF.  | Nighttime OH $\sim 7 \times 10^5 \text{ cm}^{-3}$ and nighttime HO <sub>2</sub> $\sim 8 \times 10^6 \text{ cm}^{-3}$ .<br>Increase in HO <sub>x</sub> after midnight attributed to increase in O <sub>3</sub> due to<br>transport. O <sub>3</sub> + alkenes main source of nighttime HO <sub>x</sub> .  | Ren et al. (2003a);<br>Ren et al. (2003b)            |

|   |   |  |  |
|---|---|--|--|
| Mace Head, NAMBLEX, 2002                            | Measurements: HO <sub>x</sub> measured by LIF; NO <sub>3</sub> measured by DOAS. Modelling: Zero-dimensional box models constrained to measured species, based on MCM.  | Nighttime HO <sub>2</sub> = 2–3 × 10 <sup>7</sup> cm <sup>-3</sup> ; OH below detection limit (6 × 10 <sup>4</sup> cm <sup>-3</sup> ). Model overestimated HO <sub>2</sub> . On average, O <sub>3</sub> + alkene reactions contributed 59 % and NO <sub>3</sub> + alkene reactions contributed 41 % to RO <sub>2</sub> production at night, but NO <sub>3</sub> and RO <sub>2</sub> concentrations were always higher in semi-polluted air masses than in clean marine air masses and NO <sub>3</sub> reactions dominated in these conditions. | Fleming et al. (2006); Smith et al. (2006); Sommariva et al. (2007)    |
| Writtle, London, TORCH, 2003                        | Measurements: HO <sub>x</sub> measured by LIF, RO <sub>2</sub> measured by PERCA, during a heatwave/pollution episode. Modelling: zero-dimensional box model constrained to measured species.   | OH and HO <sub>2</sub> observed above the limit of detection on several nights. OH peaked at 8.5 × 10 <sup>5</sup> cm <sup>-3</sup> ; HO <sub>2</sub> peaked at 1 × 10 <sup>8</sup> cm <sup>-3</sup> . Model overpredicted nighttime OH and HO <sub>2</sub> on average by 24 % and 7 %; underpredicted [HO <sub>2</sub> +ΣRO <sub>2</sub> ] by 22 %.   | Lee et al. (2006); Emmerson et al. (2007); Emmerson and Carslaw (2009) |
| Mexico City, MCMA 2003                              | Measurements: HO <sub>x</sub> measured by LIF, NO <sub>3</sub> measured by DOAS. Modelling: Zero-dimensional model based on MCM v3.1, constrained to measured species.  | Polluted city location characterized by high levels of NO, NO <sub>2</sub> and O <sub>3</sub> . Maximum nighttime OH ~ 1 × 10 <sup>6</sup> cm <sup>-3</sup> ; maximum nighttime HO <sub>2</sub> ~ 6 pptv. Nighttime production of radicals dominated by O <sub>3</sub> + alkene reactions (76–92 %); NO <sub>3</sub> + alkene plays a minor role. Daytime radical production ~ 25 times higher than night.   | Shirley et al. (2006); Sheehy et al. (2010); Volkamer et al. (2010)    |
| New York City, PMTACS-NY winter 2004                | Measurements: HO <sub>x</sub> measured by LIF. Modelling: Zero-dimensional model based on RACM and constrained by measurements.   | Mean maximum OH = 0.05 pptv; mean maximum HO <sub>2</sub> = 0.7 pptv. Model under-prediction of HO <sub>2</sub> was pronounced when NO was high. O <sub>3</sub> + alkene reactions were dominant nighttime source.   | Ren et al. (2006)  |
| Gulf of Maine, Northeast United States, NEAQS, 2004 | Measurements: NO <sub>3</sub> and N <sub>2</sub> O <sub>5</sub> measured by CRDS. Modelling: Zero-dimensional model based on MCM v3.1, constrained to measured species. No measurements of OH, HO <sub>2</sub> , or RO <sub>2</sub> . | Ship-based measurements onboard <i>RV Ronald H. Brown</i> in the Gulf of Maine, influenced by unpolluted marine air masses and polluted air masses from USA and Canada. Maximum modelled nighttime HO <sub>2</sub> = 7.0 × 10 <sup>8</sup> cm <sup>-3</sup> . Base model overestimated NO <sub>3</sub> and NO <sub>2</sub> observations by 30–50 %. In anthropogenic air masses reaction with VOCs and RO <sub>2</sub> each accounted for 40 % of modelled NO <sub>3</sub> loss.   | Sommariva et al. (2009)  |
| Houston, Texas, TexAQS, 2006                        | Measurements: NO <sub>3</sub> and N <sub>2</sub> O <sub>5</sub> measured by CRDS, VOCs measured by CIMS, GC, and PTRMS. No direct measurements of OH, HO <sub>2</sub> ,   | Loss rates and budgets of NO <sub>3</sub> and highly reactive VOCs calculated. NO <sub>3</sub> primarily lost through reaction with VOCs. VOC oxidation dominated by NO <sub>3</sub> , which was 3–5 times more important than O <sub>3</sub> .  | Brown et al. (2011)  |

or RO<sub>2</sub>.

|   |   |  |   |
|---|---|--|---|
| Pearl River Delta, China, PRIDE-PRD, 2006 | Measurements: HO <sub>x</sub> measured by LIF; OH reactivity measured by laser-flash photolysis and LIF; VOCs measured by FTIR and GC. Modelling: Box model based on RACM and the Mainz Isoprene Mechanism, and constrained by measurements.              | Rural site 60 km downwind of large urban region (Guangzhou), with low local wind speeds favouring accumulation of air pollutants. Maximum nighttime OH (hourly average) = $5 \times 10^6 \text{ cm}^{-3}$ ; maximum nighttime HO <sub>2</sub> (hourly average) = $1 \times 10^9 \text{ cm}^{-3}$ . Unknown recycling mechanism required for the model to reproduce measured nighttime values. OH reactivity peaked at night. Missing nighttime reactivity attributed to unmeasured secondary organic compounds.  | Lou et al. (2010);<br>Lu et al. (2012);<br>Lu et al. (2013) |
| Beijing, CAREBEIJIN G2006, 2006           | Measurements: HO <sub>x</sub> measured by LIF; OH lifetime measured by laser flash photolysis and LIF; VOCs measured by GC. Modelling: Box model based on RACM and the Mainz Isoprene Mechanism, and constrained by measurements.                         | Suburban rural site south of Beijing, under the influence of slowly moving, aged polluted air from the south. OH reactivity peaked at night. Model generally underestimated observed nighttime OH concentrations.  | Lu et al. (2013);<br>Lu et al. (2014)                       |
| Cape Verde, RHaMBLe, 2007                 | Measurements: HO <sub>x</sub> measured by LIF. Modelling: Box model based on MCM with added halogen chemistry scheme, constrained to measurements of long-lived species.  | Clean tropical Atlantic measurement site with occasional continental influence. OH was not measured at night. HO <sub>2</sub> was detected on two nights, up to $2.5 \times 10^7 \text{ cm}^{-3}$ . Model underprediction of HO <sub>2</sub> was significantly reduced by constraining the model to 100 pptv of peroxy acetyl nitrate (PAN) at night.  | Whalley et al. (2010)                                       |
| Huelva, Spain, DOMINO, 2008               | Measurements: [HO <sub>2</sub> +RO <sub>2</sub> ] measured by DUALER; HO <sub>x</sub> measured by LIF; NO <sub>3</sub> and N <sub>2</sub> O <sub>5</sub> measured by OA-CRD; OH reactivity measured by CRM-PTR-MS. No measurements of anthropogenic VOCs. | Coastal forested site with strong urban-industrial and weak biogenic influences. Maxima in [HO <sub>2</sub> +RO <sub>2</sub> ] and [HO <sub>2</sub> ] were observed around noon and midnight. Enhanced nighttime [HO <sub>2</sub> +RO <sub>2</sub> ] (up to 80 pptv) was observed in air masses from the urban-industrial region. Maximum nighttime HO <sub>2</sub> = 8 pptv. Measured NO <sub>3</sub> was generally below LOD; calculated NO <sub>3</sub> up to 20 pptv. Calculated production of RO <sub>2</sub> from NO <sub>3</sub> +alkenes accounts for 47–54 % of observed [HO <sub>2</sub> +RO <sub>2</sub> ]. Ozonolysis of unmeasured alkenes could account for remaining [HO <sub>2</sub> +RO <sub>2</sub> ]. | Andrés-Hernández et al. (2009)                              |



7 Table 2. Details of supporting measurements.

| Species  | Instrument, Technique  | Time resolution; Limit of detection (LOD)  | References  |
|--|--|--|---|
| CO   | Aero Laser AL5002 Fast Carbon Monoxide Monitor. Excitation and fast response fluorescence at $\lambda = 150$ nm.   | 1 s; 3.5 ppbv  | Gerbige et al. (1999)                                 |
| O <sub>3</sub>   | Thermo Scientific TEi49C Ozone analyser. Absorption spectroscopy at $\lambda = 254$ nm.  | 1 s; 0.6 ppbv  | Hewitt et al. (2010)                                  |
| NO, NO <sub>2</sub> , NO <sub>x</sub><br>(NO + NO <sub>2</sub> ) | Air Quality Design dual channel fast-response NO <sub>x</sub> instrument. Chemiluminescence from NO + O <sub>3</sub> reaction. Conversion of NO <sub>2</sub> to NO by photolysis.  | 10 s; 3 pptv for NO, 15 pptv for NO <sub>2</sub>   | Stewart et al. (2008)                                 |
| NO <sub>2</sub> , $\Sigma$ ANs, $\Sigma$ PNs                     | TD-LIF (thermal dissociation laser induced fluorescence). Detection of NO <sub>2</sub> by laser-induced fluorescence. Thermal decomposition of $\Sigma$ ANs (total alkyl nitrate) and $\Sigma$ PNs (total peroxy nitrate) to NO <sub>2</sub> . | 1 s; 9.8 pptv for NO <sub>2</sub> , 28.1 pptv for $\Sigma$ ANs, 18.4 pptv for $\Sigma$ PNs       | Dari-Salisburgo et al. (2009); Di Carlo et al. (2013) |
| Alkenes  | Whole air samples (WAS) analysed by laboratory-based gas chromatography with flame ionization detection (GC-FID).  | Typically 30 s; variable limits of detection   | Hopkins et al. (2003)                                 |
| NO <sub>3</sub> , N <sub>2</sub> O <sub>5</sub>                  | BBCEAS (broadband cavity-enhanced absorption spectroscopy) of NO <sub>3</sub> at $\lambda = 642$ – $672$ nm. N <sub>2</sub> O <sub>5</sub> measured following thermal dissociation to NO <sub>3</sub> + NO <sub>2</sub> .                      | 1 s; 1.1 pptv for NO <sub>3</sub> , 2.4 pptv for NO <sub>3</sub> + N <sub>2</sub> O <sub>5</sub> | Kennedy et al. (2011)                                 |
| HCHO   | Hantzsch technique: Liquid-phase reaction of formaldehyde followed by excitation, and fluorescence of resulting adduct at $\lambda = 510$ nm.  | 60 s; 81 pptv  | Still et al. (2006)                                   |

8 Table 3. Mean mixing ratios of selected gas phase species, and air temperature, measured during  
9 RONOCO and SeptEx. The flight and season during which the maximum values were measured  
10 are given in parentheses. NO<sub>2</sub> data are from the TD-LIF instrument. Zero values indicate  
11 measurements below the limit of detection.

| Species                | Summer RONOCO | SeptEx | Winter RONOCO | Maximum              |
|------------------------|---------------|--------|---------------|----------------------|
| CO / ppbv              | 102.3         | 117.1  | 139.3         | 256.0 (B537, summer) |
| O <sub>3</sub> / ppbv  | 39.6          | 40.4   | 38.6          | 89.8 (B537, summer)  |
| NO <sub>3</sub> / pptv | 21.1          | 0      | 6.2           | 176.9 (B537, summer) |
| NO / ppbv              | 0.05          | 0      | 0             | 18.9 (B539, summer)  |
| NO <sub>2</sub> / ppbv | 1.6           | 1.7    | 2.3           | 18.6 (B568, winter)  |
| Temperature / K        | 286.5         | 286.2  | 276.4         | 297.5 (B537, summer) |

12 Table 4. Combined daytime and nighttime mean concentrations of OH and mean mixing ratios of  
 13 HO<sub>2</sub>\* with the FAGE instrument's average 1σ limits of detection for a 5 minute averaging period  
 14 during the RONOCO and SeptEx fieldwork.

|        | OH / molecule cm <sup>-3</sup> |                    | HO <sub>2</sub> * / pptv |                    |
|--------|--------------------------------|--------------------|--------------------------|--------------------|
|        | Mean concentration             | Limit of detection | Mean mixing ratio        | Limit of detection |
| Summer |                                | $1.8 \times 10^6$  | 1.6                      | 0.03               |
| SeptEx | $1.8 \times 10^6$              | $1.2 \times 10^6$  | 2.9                      | 0.02               |
| Winter |                                | $6.4 \times 10^5$  | 0.7                      | 0.02               |

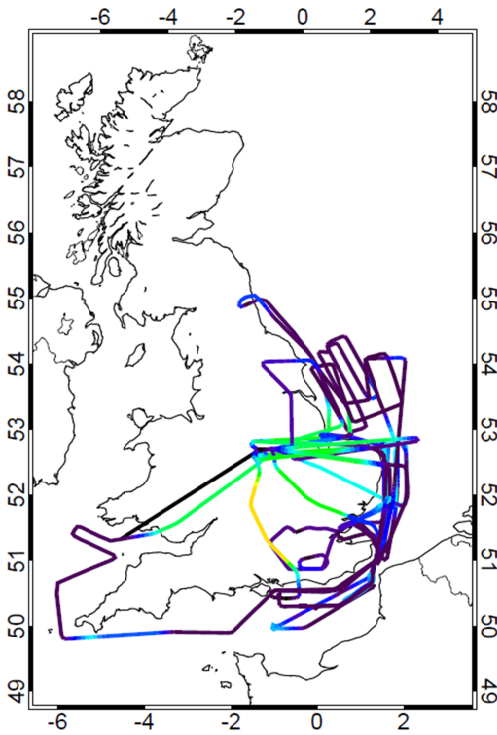
15 Table 5. Mean and, in parentheses, maximum HO<sub>2</sub>\* mixing ratios measured during RONOCO  
 16 and SeptEx.

|       | Mean (maximum) HO <sub>2</sub> * mixing ratio / pptv |              |             |
|-------|--|--------------|-------------|
|       | Summer   | SeptEx       | Winter      |
| Dawn  | 0.74 (1.19)  |              | 0.54 (1.81) |
| Day   |  | 3.78 (11.79) | 0.49 (1.68) |
| Dusk  | 2.73 (9.97)  |              | 0.32 (0.97) |
| Night | 1.86 (13.58)   |              | 0.98 (2.02) |

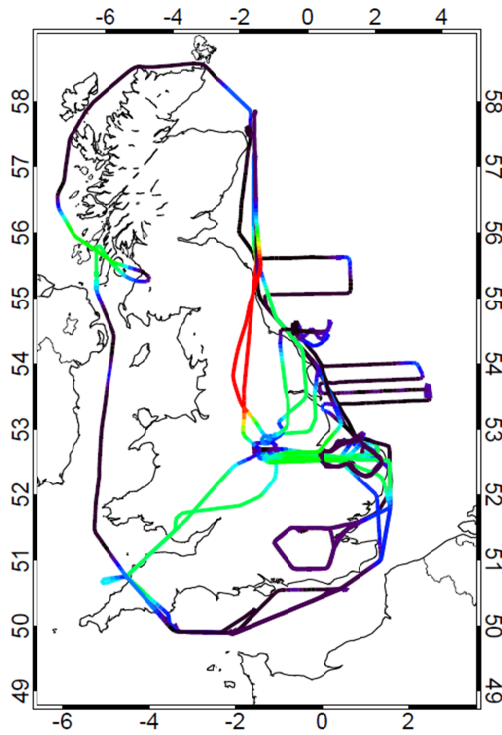
17 Table 6. Average rates of instantaneous production of HO<sub>2</sub> from reactions of O<sub>3</sub> and NO<sub>3</sub> with  
 18 alkenes.

| Measurements    | HO <sub>2</sub> production rate ( $\Sigma P_{\text{HO}_2}$ ) / 10 <sup>4</sup> molecule cm <sup>-3</sup> s <sup>-1</sup> |     |      |       |
|-----------------|--|-----|------|-------|
|                 | Dawn   | Day | Dusk | Night |
| Summer          |  |     |      |       |
| NO <sub>3</sub> | 0  |     | 2.8  | 3.8   |
| O <sub>3</sub>  | 0.5  |     | 2.2  | 1.7   |
| Total           | 0.5  |     | 5.0  | 5.5   |
| Winter          |  |     |      |       |
| NO <sub>3</sub> | 0.4  | 0.4 | 0.4  | 0.5   |
| O <sub>3</sub>  | 1.4  | 1.5 | 1.2  | 1.2   |
| Total           | 1.8  | 1.9 | 1.6  | 1.7   |

(a) Summer RONOCO



(b) SeptEx



(c) Winter RONOCO

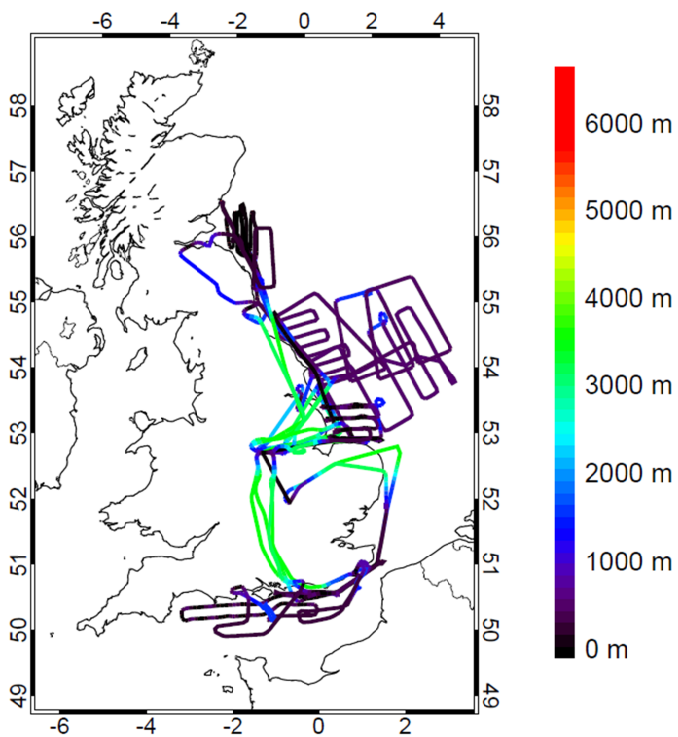
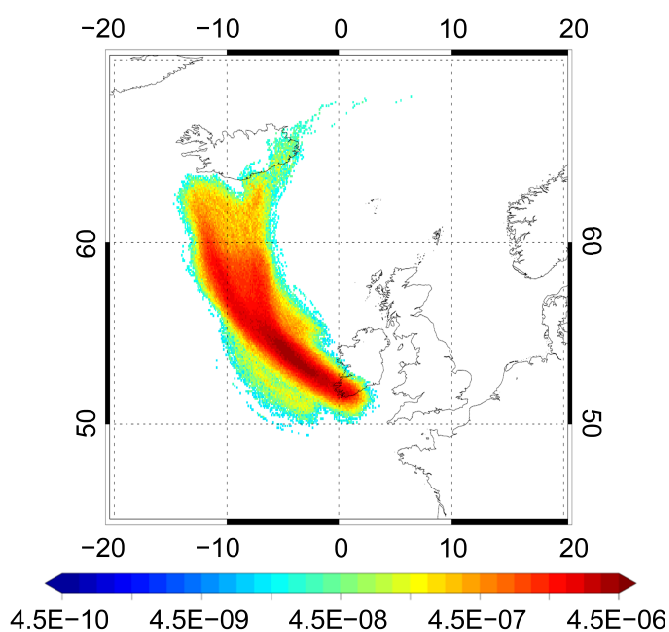
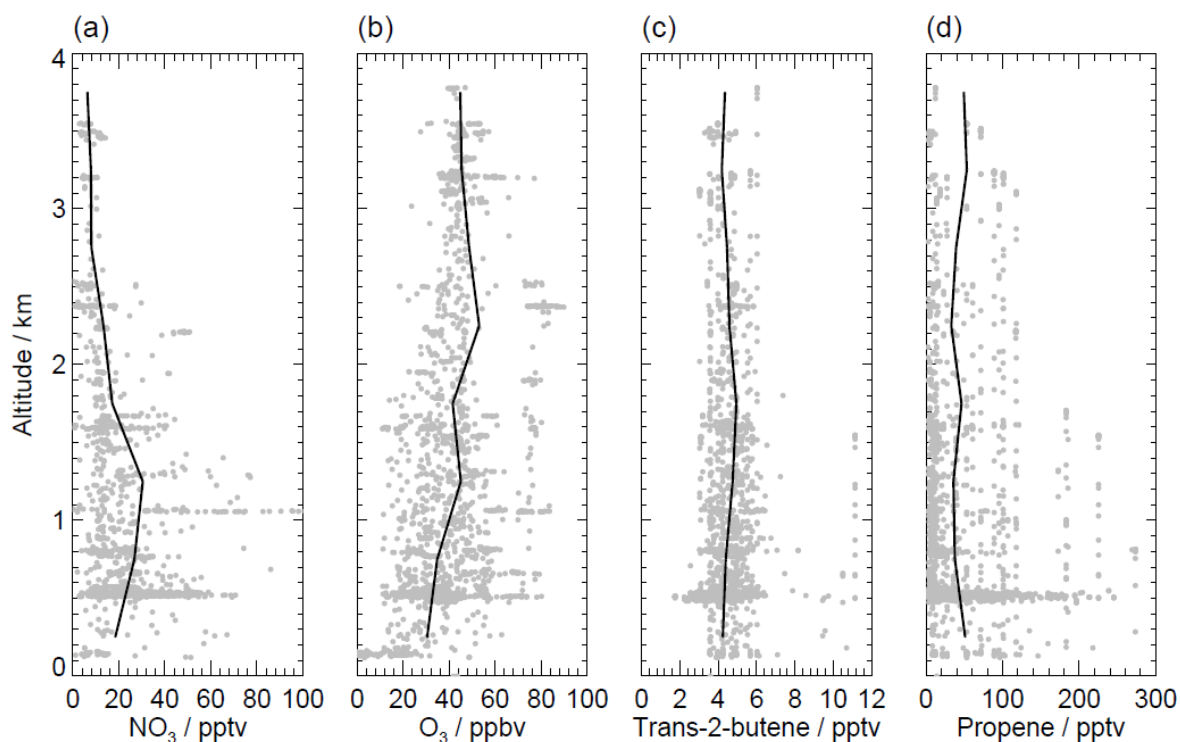


Figure 1. Flight paths for: (a) Summer RONOCO, (b) SeptEx, and (c) winter RONOCO measurement campaigns, coloured by altitude.



4  
11 Figure 2. Footprint map for flight B535 on 17<sup>th</sup> July 2010, showing model particle densities (g  
12 s m<sup>-3</sup>) in a 300 m deep layer from the surface, integrated over a 24 hour period beginning 48  
13 hours prior to the flight.



8  
12 Figure 3. Nighttime altitude profiles of a) NO<sub>3</sub>; b) O<sub>3</sub>; c) *trans*-2-butene; d) propene, showing  
13 60 second data (grey points) and mean values in 500 m altitude bins (solid black lines).

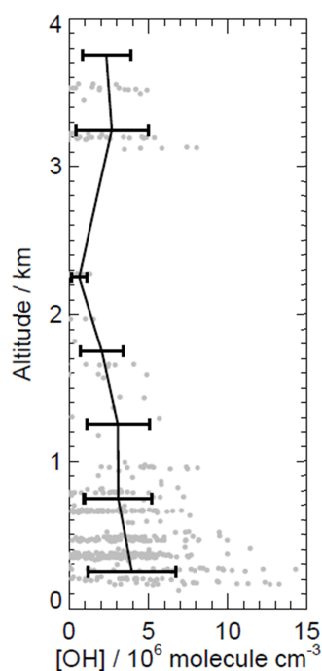


Figure 4. Altitude profile of OH measured during SeptEx showing 60 second data (grey points) and mean values in 500 m altitude bins (solid black lines). Error bars are  $1\sigma$ .

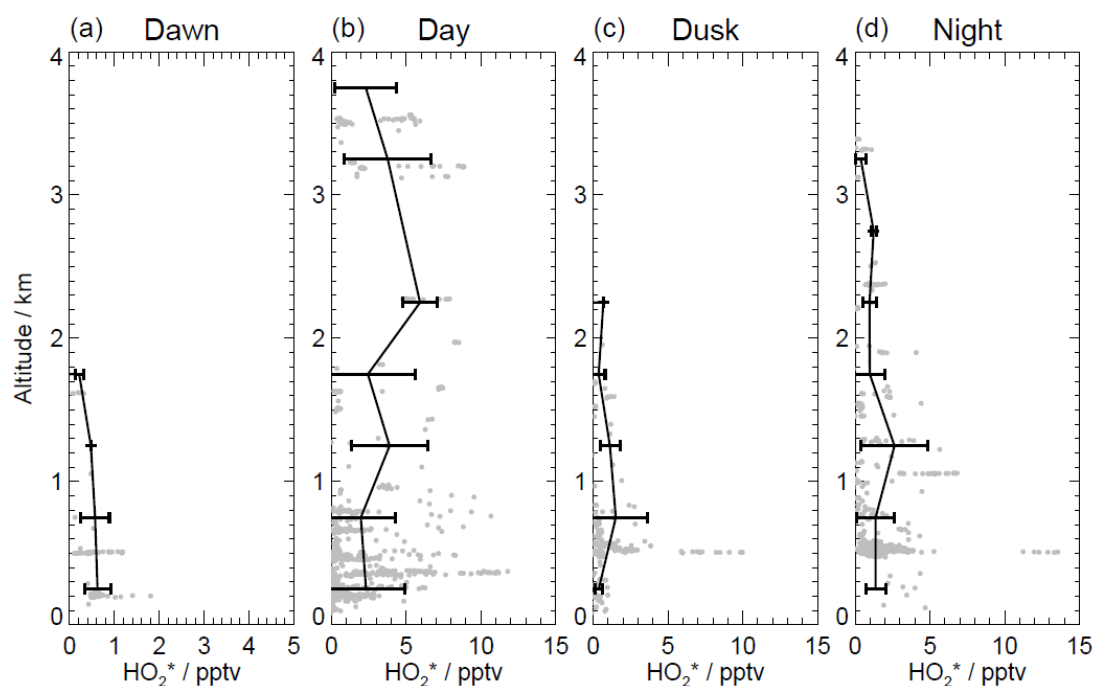


Figure 5. Altitude profiles of  $\text{HO}_2^*$  measured in RONOCO and SeptEx during: a) dawn; b) day; c) dusk; d) night, showing 60 second data (grey points) and mean values in 500 m altitude bins (solid black lines). Error bars are  $1\sigma$ .



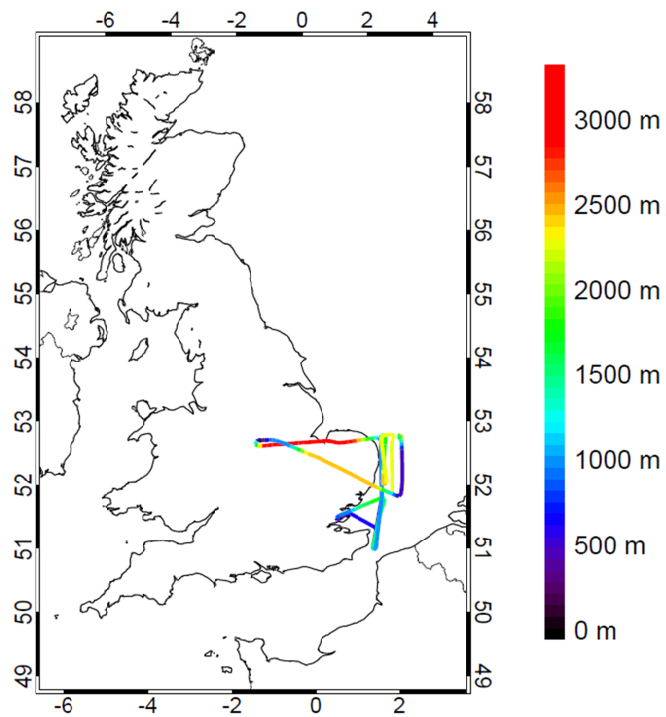
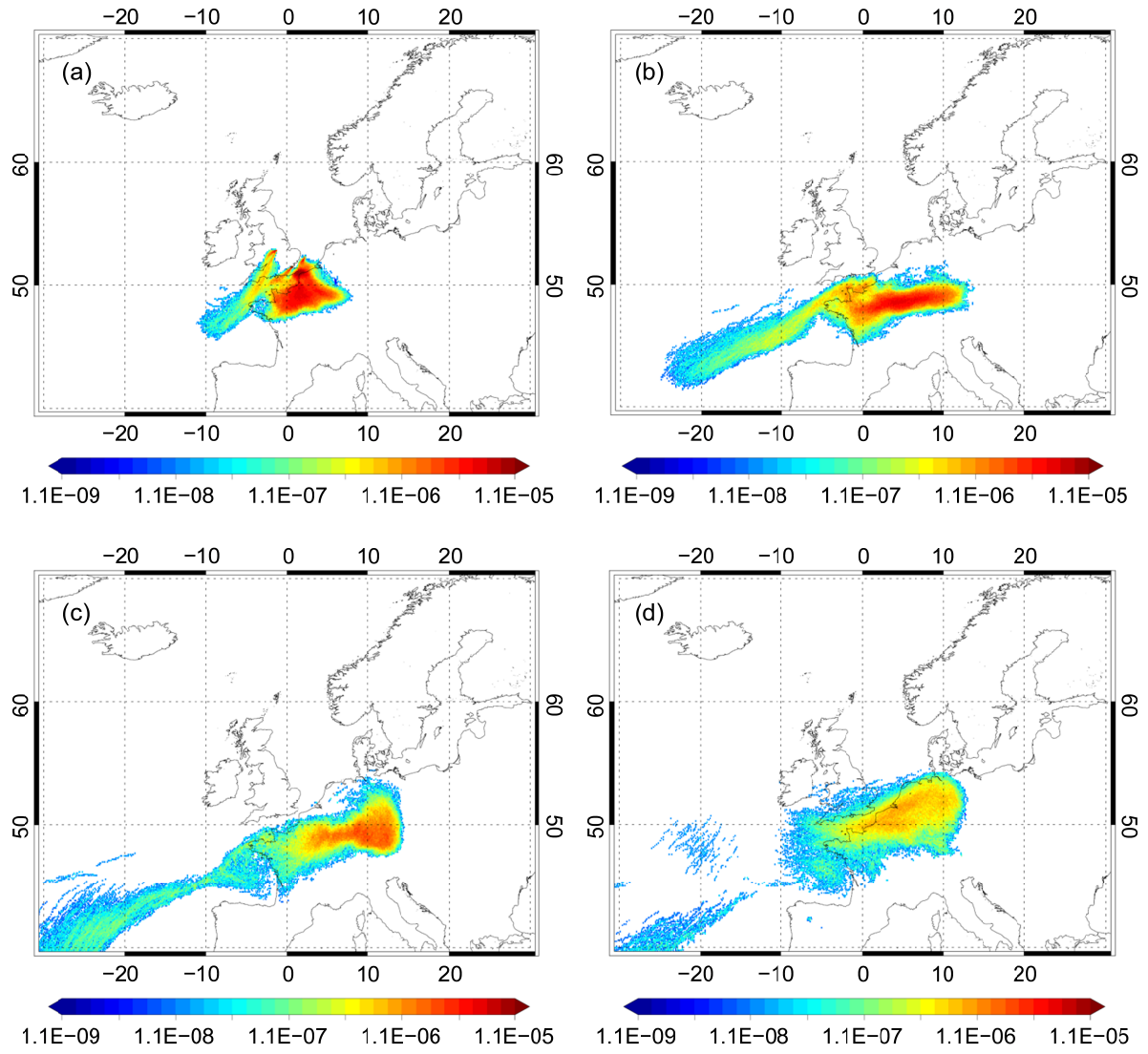
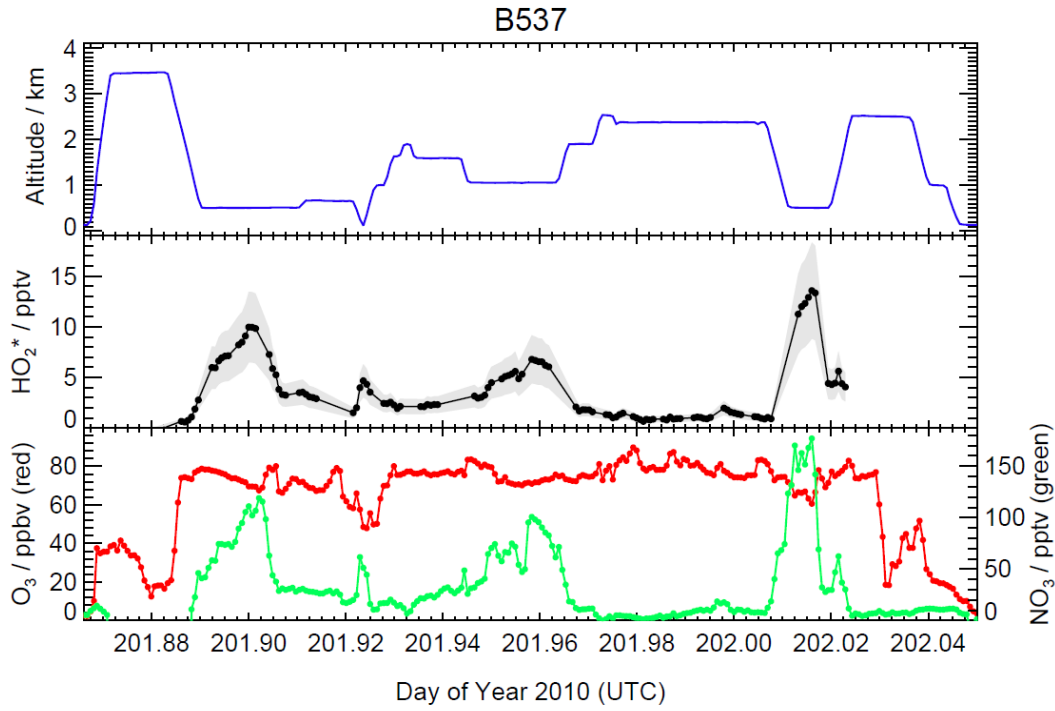


Figure 6. Flight track of flight B537 on 20<sup>th</sup> July 2010, coloured by altitude.



4

11 Figure 7. Footprint maps for flight B537 on 20<sup>th</sup> July 2010, showing model particle densities  
 12 ( $\text{g s m}^{-3}$ ) in a 300 m deep layer from the surface, integrated over 24 hour periods beginning  
 13 (a) 24 hours, (b) 48 hours, (c) 72 hours, and (d) 96 hours prior to the flight.

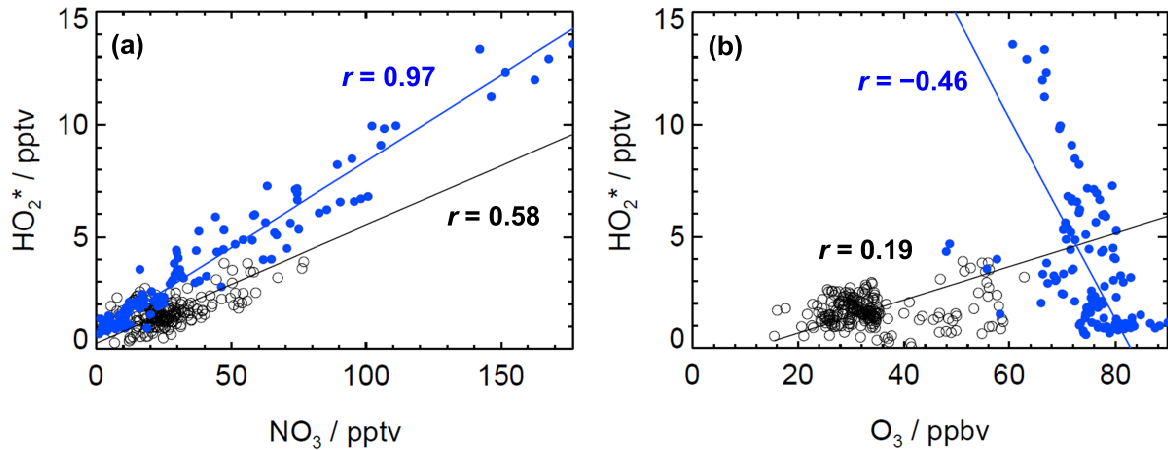


5

12 Figure 8. Time series of altitude (top panel, blue),  $\text{HO}_2^*$  (middle panel, black, with grey  
 13 shading representing the uncertainty in the measurements),  $\text{O}_3$  (bottom panel, red) and  $\text{NO}_3$   
 14 (bottom panel, green) during nighttime flight B537 on 20<sup>th</sup> July 2010.

9

10



11

15 Figure 9.  $\text{HO}_2^*$  versus (a)  $\text{NO}_3$  and (b)  $\text{O}_3$  during flight B537 (blue, filled circles) and during  
 16 all other nighttime flights (black, open circles). The solid lines are lines of best fit to the data.

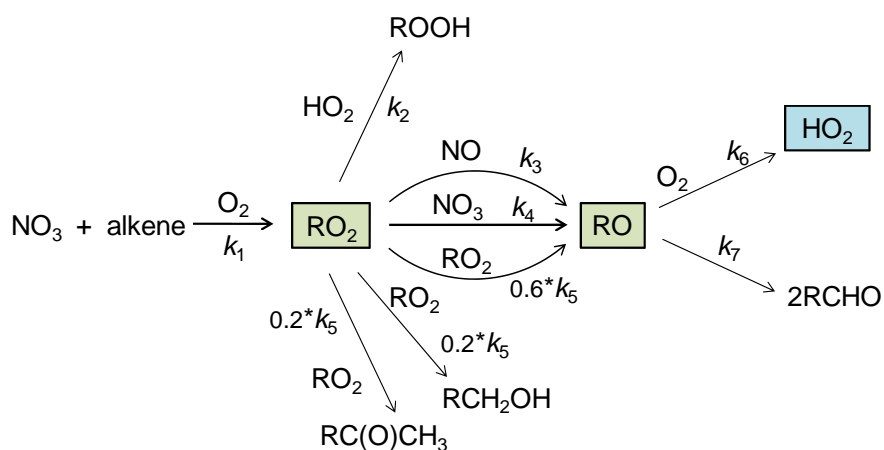


Figure 10. Generalised reaction scheme for production of  $\text{RO}_2$  and  $\text{HO}_2$  following reaction of  $\text{NO}_3$  with an alkene.

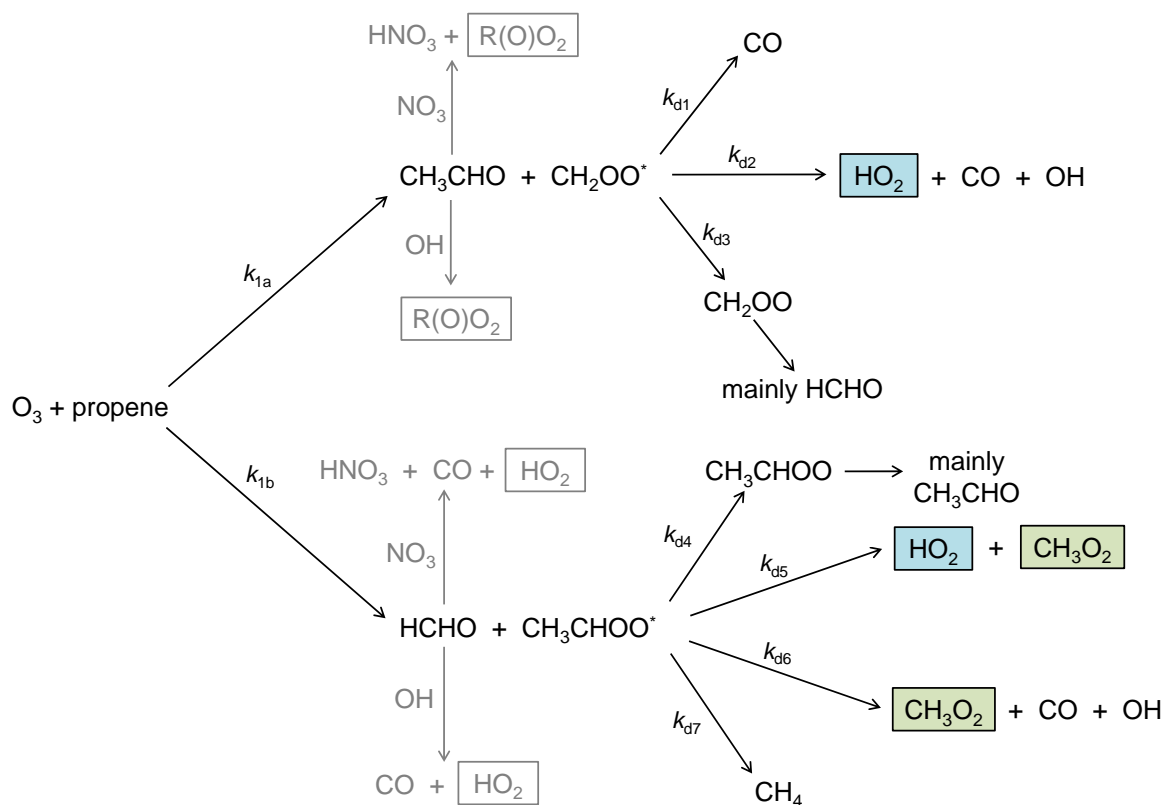
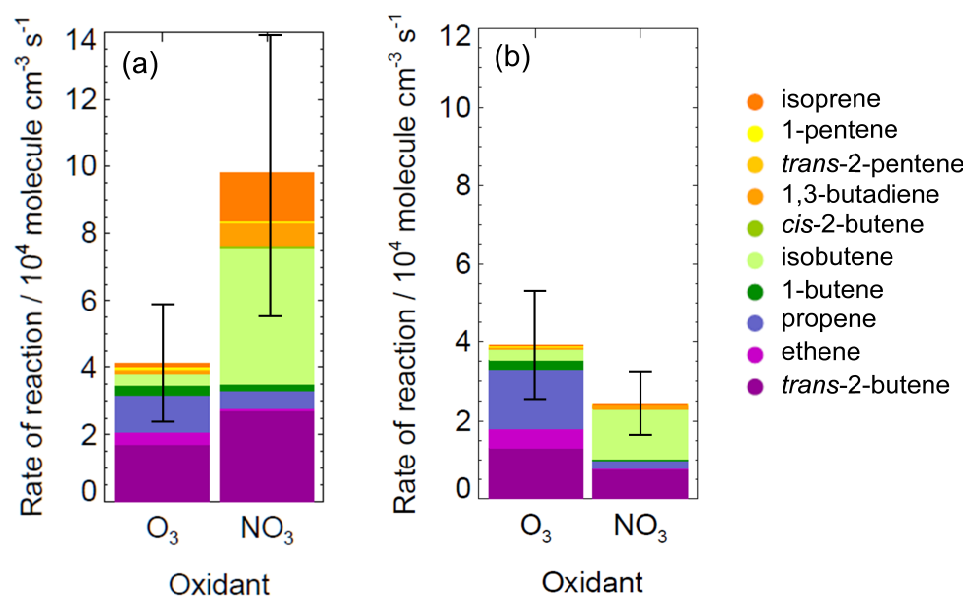


Figure 11. Reaction scheme for  $\text{O}_3 + \text{propene}$ , showing production of  $\text{HO}_2$  and the methyl peroxy radical,  $\text{CH}_3\text{O}_2$ .



4  
 11 Figure 12. Average nighttime rates of reaction between  $O_3$ , and  $NO_3$  with alkenes during: a)  
 12 summer; and b) winter RONOCO flights. Error bars represent the combined uncertainty in the  
 13 measurements.

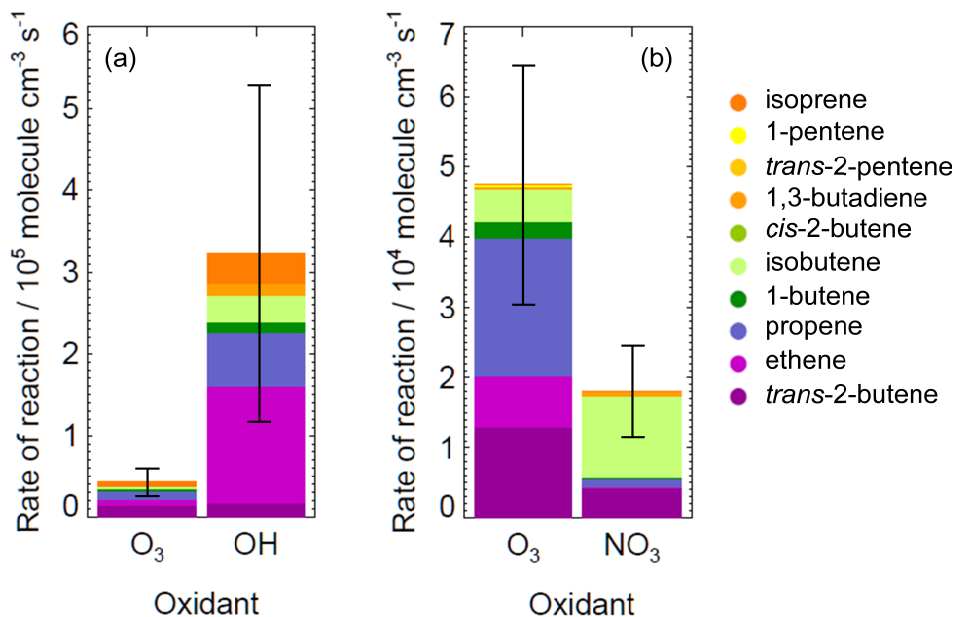


Figure 13. Average daytime rates of reaction of (a)  $O_3$  and OH with alkenes during SeptEx; and (b)  $O_3$  and  $NO_3$  with alkenes during winter. Note the different scales.  $NO_3$  was not detected during daytime SeptEx flights ( $LOD = 1.1 \text{ pptv}$ ); OH was not detected during daytime winter flights ( $LOD = 6.4 \times 10^5 \text{ molecule cm}^{-3}$ ). Error bars represent the combined uncertainties in the measurements.

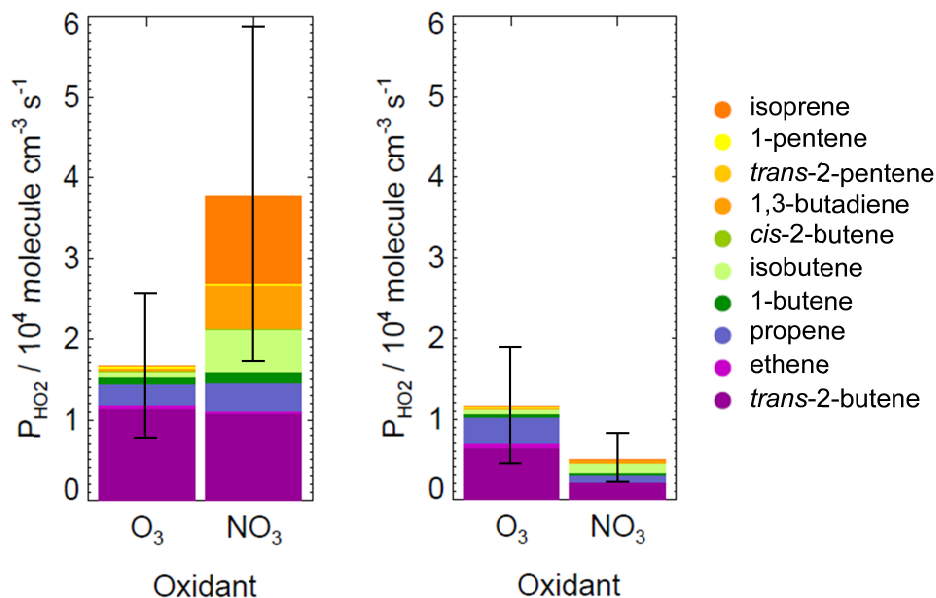


Figure 14. Average rates of instantaneous production of  $HO_2$  from reactions of  $O_3$  and  $NO_3$  with alkenes during: a) summer; and b) winter RONOCO flights. Error bars represent the combined uncertainty in the measurements.

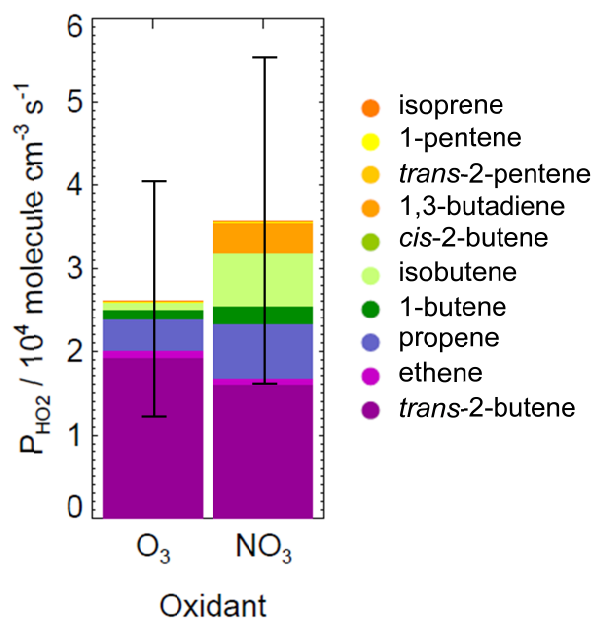


Figure 15. Average rates of instantaneous production of  $\text{HO}_2$  from reactions of  $\text{O}_3$  and  $\text{NO}_3$  with alkenes during flight B537. Error bars represent the combined uncertainty in the measurements.

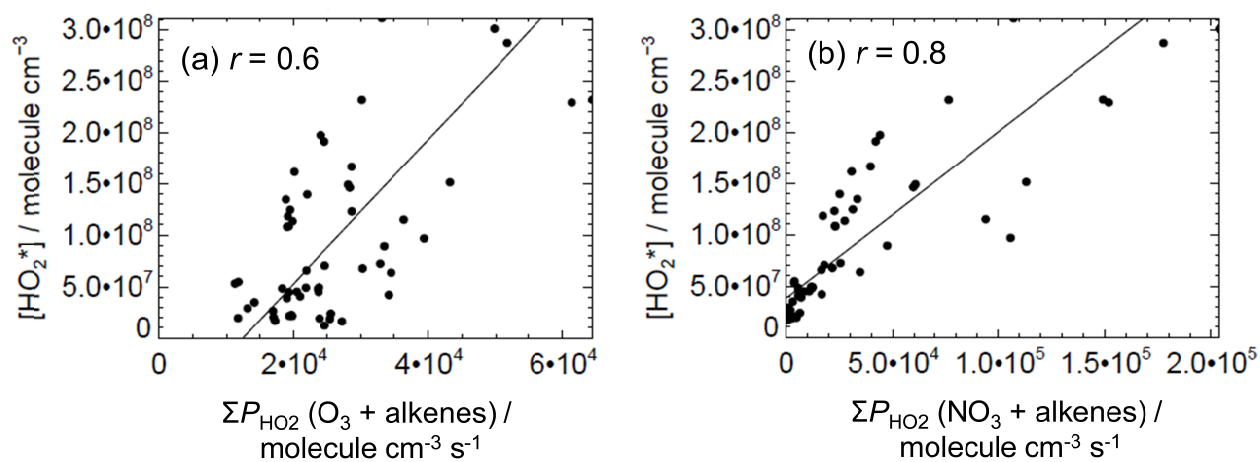


Figure 16.  $[\text{HO}_2^*]$  versus total rate of instantaneous production of  $\text{HO}_2$  from reactions of: a)  $\text{O}_3$ ; and b)  $\text{NO}_3$  during flight B537. Correlation coefficients ( $r$ ) are given in each plot. Solid lines are lines of best fit to the data.